UNIVERSITY OF OKLAHOMA

GRADUATE COLLEGE

GEOLOGICAL AND GEOPHYSICAL ANALYSIS OF STRUCTURAL AND STRATIGRAPHIC CHARACTERISTICS OF POST MISSISSIPPIAN AGE SEDIMENTS WITHIN THE NORTHEASTERN FORT WORTH BASIN, TX AND THEIR BASIN SCALE SIGNIFICANCE

A THESIS

SUBMITTED TO THE GRADUATE FACULTY

in partial fulfillment of the requirements for the

Degree of

MASTER OF SCIENCE

By

RACHEL PETIT
Norman, Oklahoma
2015

GEOLOGICAL AND GEOPHYSICAL ANALYSIS OF STRUCTURAL AND STRATIGRAPHIC CHARACTERISTICS OF POST MISSISSIPPIAN AGE SEDIMENTS WITHIN THE NORTHEASTERN FORT WORTH BASIN, TX AND THEIR BASIN SCALE SIGNIFICANCE

A THESIS APPROVED FOR THE
CONOCOPHILIPS SCHOOL OF GEOLOGY AND GEOPHYSICS

BY

____
Dr. Jamie Rich, Co-Chair

____
Dr. Kurt J. Marfurt, Co-Chair

____
Dr. John D. Pigott

I would like to dedicate this thesis to my family and my beloved Fiancé Tom. They have been here, helping and supporting me through the stressful times and through the good times as well. Graduate School has been one of my best experiences, and I am grateful for the support of all the people around me.

Acknowledgements

I would like to thank the professors at the University of Oklahoma for their support with the analysis of my thesis data: Dr. Rich for his help with identifying the formations within the survey, Dr. Marfurt for his help teaching me how to use Petrel and interpretation, and Mike Ammerman, of Ammerman Geophysical Consulting, Devon and previously Mitchell Energy for his advice and suggestions.

I would also like to thank the PHD students who assisted me with the first draft of my thesis: Bo Zhang and especially Tengfei Lin. I thank Abdulmohsen AlAli and Sumit Verma for their assistance with the constructing synthetic seismograms.

Additionally I would like to thank the AASPI Consortium for the use of the AASPI software, Schlumberger for the use of the Petrel software, and Devon Energy for the donation of a license to the seismic and well data.

I would finally like to thank the University of Oklahoma for its support and funding.

Table of Contents

List of Figures

Abstract

The Fort Worth Basin has been an important source of oil and gas since the early 1900s when oil was discovered while drilling for water. Mitchell Energy drilled the first gas discoveries within the Barnett Shale in 1981. From the 1990s onward, the Barnett Shale, both a source rock and unconventional reservoir, has been the main focus of exploration within the basin. Much of the literature focuses on the layers within the basin that affect the productivity of the Barnett. Due to the lack of economic interest in the shallower layers, there exists little literature examining these strata.

The most tectonically complex events occurred just at the end of Marble Falls Limestone deposition when the Ouachita Orogeny caused extensive faulting, depositional shifts and subsidence through the Pennsylvanian. This study focuses on an analysis of the geologic and geophysical expressions of the events before, during and after the Ouachita Orogeny. Mitchell Energy acquired wide azimuth long offset seismic data in 1999 just west of the highly productive Newark East Field to further the expanding exploration of the Barnett Shale. Before the formation of the basin, faults in the northeastern portion of the basin were related to the basement Mineral Wells Fault System, including those occurring within the survey. The regional faults were reactivated by the advancing Ouachita Thrust Front. Examination of fluvial channels and clinoforms illustrate westward shifts in deposition as the basin formed. Buried caves within the Ellenburger Limestone collapsed under the overburden of Pennsylvanian age deposition. Thickness maps of the formations illustrate the timing of the karst collapse and fault reactivations. The large-scale tectonic events are cataloged in the rock layers within the survey.

Chapter 1: Introduction

Hydrocarbons were first discovered in the Fort Worth Basin in the early 1990s while drilling for water. Since then, the basin has become an important source of oil and gas in the United States. Production from conventional reservoirs peaked in 1971. Led by Mitchell Energy in the 1990s unconventional sources of oil and gas began to become a reality, with the Fort Worth Basin now one of the most fully developed shale gas fields in North America. Unconventional reservoirs within the basin include the Mississippian age Barnett Shale and the Early Pennsylvanian age Marble Falls Limestone. Continuous gas and oil accumulation take place within fractured shale, chalk and low permeability reservoirs. Numerous 3D seismic surveys have been collected within the Fort Worth Basin to examine the Barnett Shale. Of a secondary focus are the formations whose structure affects the production within the Barnett. Plentiful karst features characterize the Ellenburger Limestone, just beneath the Barnett Shale above the basement. These collapse chimneys extend upward, effecting production within the Barnett Shale. The Marble Falls, an unconventional limestone reservoir atop the Barnett Shale, is a subject of focus as well. However, few seismic surveys are used to examine post-Mississippian age strata.

The most influential tectonic events affecting the basin occurred beginning in the late Mississippian as Gondwana collided with Laurentia to form Pangaea. The Ouachita Orogeny accounted for much of the faulting and deformation that is present throughout the basin. Layers of Pennsylvanian age catalog fluvial shifts within the basin as well as times of erosion and uplift. The end of the Ouachita Orogeny and the opening of the Gulf of Mexico in the Jurassic led to a drastic change in the stress regime, as compression gave way to extension and the mountains began to weather away (Blakey).

Mitchell Energy was one of the first companies to pioneer production from the Barnett Shale. Several seismic surveys were collected just west of the highly productive Newark East Field to examine the effect of karsting on the Barnett Shale. In 1999 they acquired wide azimuth, long offset data and combined it with two older surveys, acquired in 1995 and 1997. The merged survey has characteristics that are consistent with basin-wide structural and stratigraphic shift.

This study focuses on an analysis of the geologic and geophysical expressions of the events before, during and after the Ouachita Orogeny.

Chapter 2: Geologic Overview

The Fort Worth Basin is a foreland basin that covers 15,000 square miles in north central Texas and is deepest in the northeastern corner against the Muenster Arch. The sedimentary sequence within the basin (Figure 1) shallows gradually to the west over the Bend Arch and pinches out sharply against the Ouachita Thrust Front on the east (Pollastro et al., 2007).

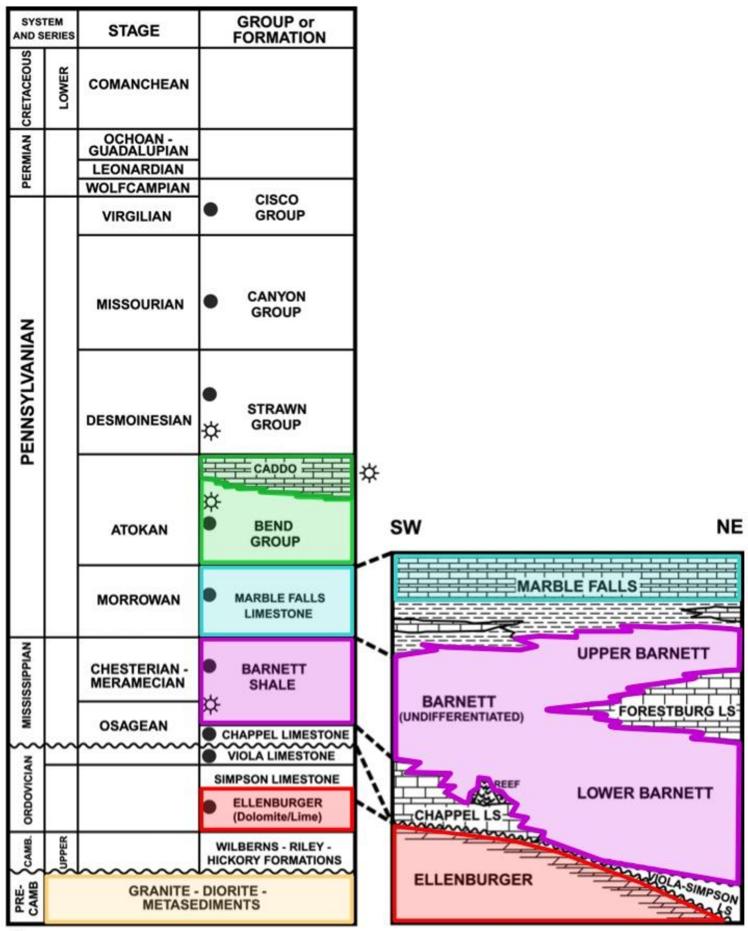

Figure 1. Stratigraphic column within the northeastern Fort Worth Basin. Color codes established on this chart will remain constant throughout the paper. From Zhao et al. (2007).

The Fort Worth Basin is an asymmetrical wedge shaped basin parallel to the

Ouachita Thrust Front (Figure 2). The western edge is defined by the Bend Arch, which formed as the basin subsided and the entire region tilted westward. The north edge is defined by the Red River and Muenster Arches, which are both Cambrian igneous fault blocks that were reactivated by the Ouachita Orogeny. Thick-skinned thrusting is common throughout the basin, but the continental collision caused thin-skinned over thrusting on the southern edge (Nicholas et al., 1975). Also at the southern edge is the Llano uplift, which is an uplifted dome of Precambrian rocks associated with the Ouachita Orogeny (Krueger et al., 1986).

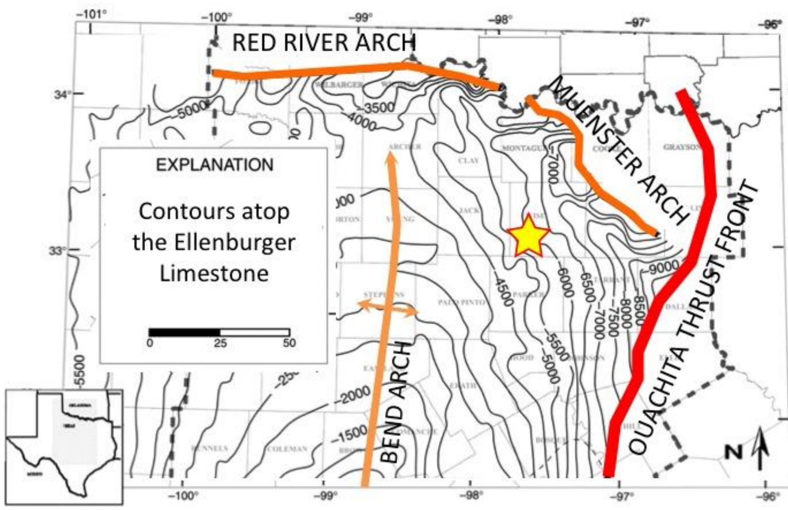

Figure 2. Structure of the Fort Worth Basin shown by structural contours at the top of the Ellenburger Limestone. The basin deepens toward the northeastern boundary. From Pollastro et al. (2007).

The Gulf Coast was a passive continental margin in the Cambrian, with sea level steadily rising up the coast, covering more and more of the continent. The Wilberns, Riley and Hickory formations were deposited in an offshore environment, with the lower units being a mix of clastics, then the upper units being mostly carbonate.

The sea level continued to rise into the Ordovician with shallow water sedimentary rock deposition along the shelf north of the Iapetus Ocean. In this widespread epeiric carbonate shelf the Ellenburger Limestone was deposited (Figure 3). The inland sea remained as nearly 400 ft of clean limestone was deposited in the region.

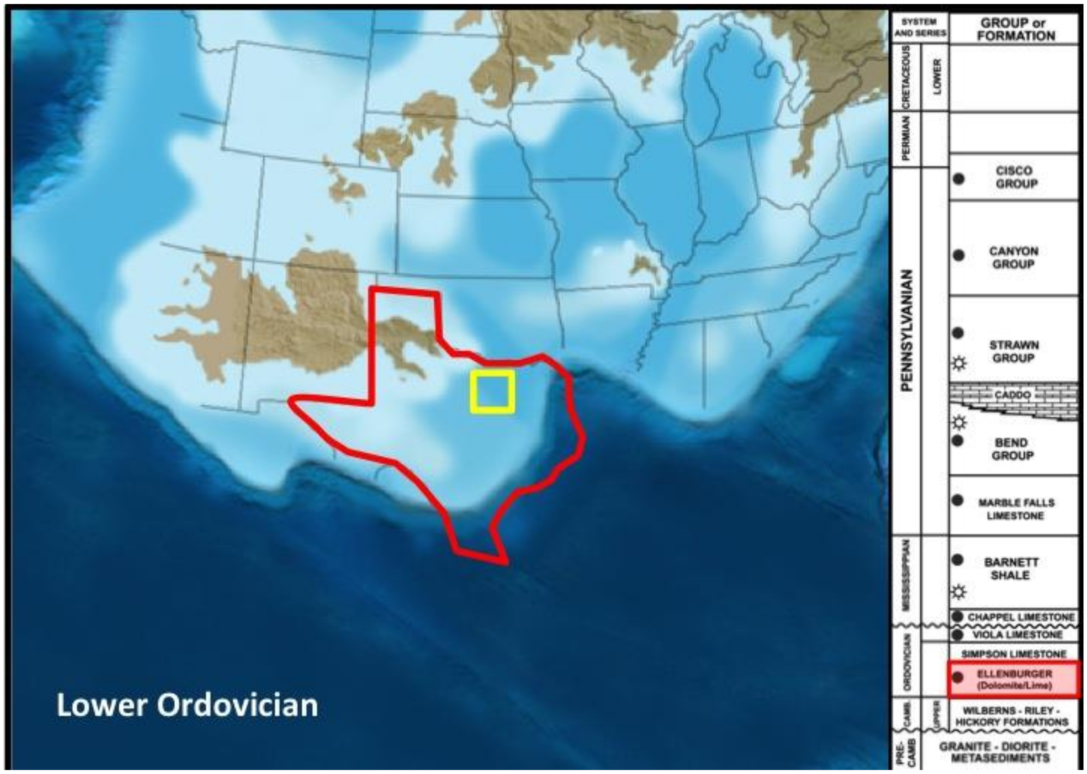

Figure 3. Depositional environment map of Texas in the Early Ordovician at the time of the Ellenburger Limestone. The tectonic environment is that of a shallow water passive margin. By Ron Blakey, Colorado Plateau Geosystems, Inc.

Sea level retreated at the end of the Ordovician, with the coast just to the east of the study area in the Silurian. Throughout the Devonian there occurred periods of sub-aerial exposure leading to erosion and several unconformities between the Ellenburger and the overlying rocks. This cycle of subaerial exposure led to an absence of Silurian and Devonian age rocks and heavy karsting of the now exposed Ordovician

Limestones. With the approach of the subduction zone off the southern coast, the collision of Laurussia and Gondwana to form Pangaea began in the late Mississippian. The Ouachita Orogeny began as these tectonic stresses thrust folded the southern margin (Pollastro et al., 2007).

The Barnett Shale was deposited from terrigenous material off the Ouachita front over the lower erosional unconformity. The Barnett shale was originally deposited over the extent of the region but later eroded to just the current basin extent. The Barnett Shale acts as the major source rock within the basin and, since 1998, an unconventional reservoir. The Barnett Shale makes an excellent source rock due to its carbon richness and volume. With an average TOC of 4%, the shale is richest in the southern part of the basin with a TOC of 12%. The kerogen is type II, with some type III mixed in (Martineau et al., 2007). The Barnett Shale is over a thousand feet thick in the northwest corner along the Muenster Arch, thinning to the east over the thrust front. The thermal maturation of the Barnett Shale took place as the basin subsided, causing it to be gas producing in the deeper eastern section and oil producing out to the west (Figure 4). In the far northeastern part of the basin, there is a layer of limestone called the Forestburg Limestone, but the layer is absent in the area of the study (Martineau et al., 2007). Overtop the Barnett shale a layer of hard, dense Chester age limestone was deposited to form a seal and fracture barrier.

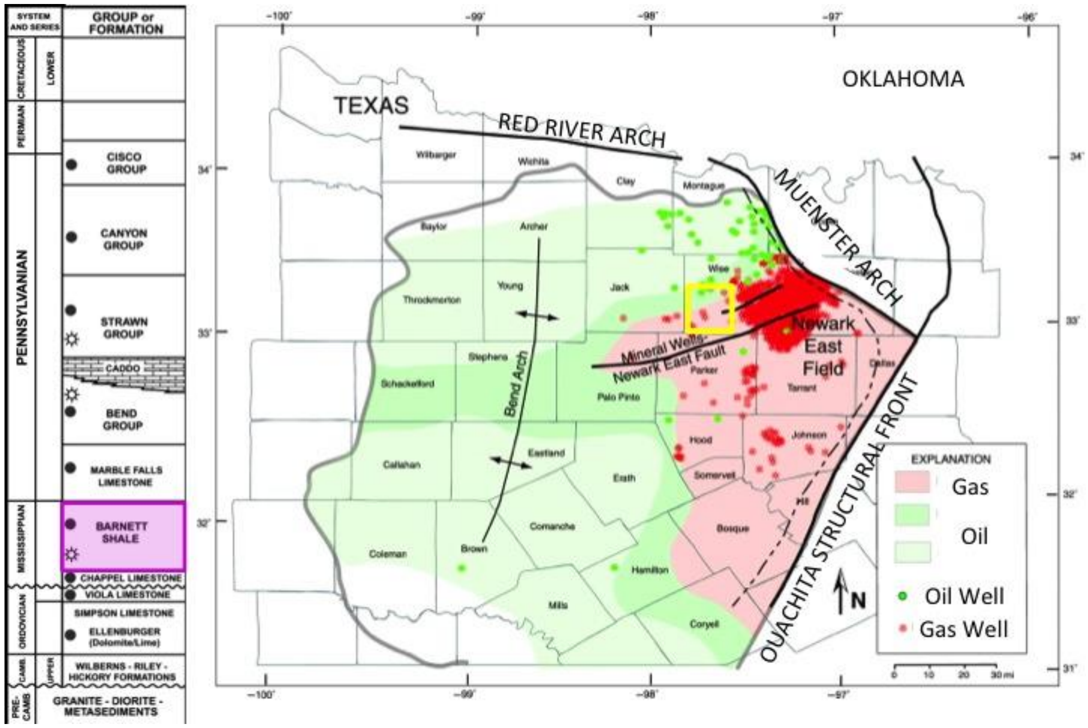

Figure 4. Gas and oil phase map within the Fort Worth Basin. The Survey is located in the southwestern corner of Wise County, just at the edge of the gas phase map. From Pollastro et al. (2007).

The end of the Mississippian marked the end of subduction and the beginning of mountain building. The Mississippian end also marked the transition of the passive continental margin deposition into an actively subsiding basin. The Ouachita Orogeny created a string of mountain fronts with associated basins from the Appalachians to Oklahoma. This trend includes the Black Warrior, Arkoma, Kerr, Val Verde and Marfa Basins (Khatiwada et al., 2013). As the collision occurred and the foredeep basin subsided, a forebulge formed at the western edge (AlKaheem et al., 2013). This subsurface high was named the Bend Arch, and served as the western edge of the basin.

The structural implications of the Ouachita Orogeny are widespread. The compression on the western edge caused the reactivation of large, basement faults creating the Muenster and Red River Arches. The Muenster Arch was uplifted to form the boundary on the northeastern side of the basin and the Red River Arch made up the northern boundary. Both are blocks of Cambrian and Mississippian age sediments atop blocks of Precambrian igneous and metamorphic sediment associated with earlier rifting. These blocks were large intrusions of Precambrian age, associated with the rifting and formation of the Southern Oklahoma Aulacogen (Krueger et al., 1986). The basin-ward edges of these blocks grade into the Fort Worth Basin as a step system of fault blocks displaced almost 1500 ft down into the basin. Both arches acted as an active sediment source throughout the Pennsylvanian, shedding arkosic sediment along the margins of the basin.

Another result of the Ouachita Orogeny was the Llano uplift and the associated Lampasas Arch. The Llano uplift acts as the southern boundary of the Fort Worth Basin. The Llano Uplift is a structural dome defined by a Precambrian age massive granitic intrusion (Krueger et al., 1986). The pluton was uplifted during the middle Pennsylvanian as the advancing Ouachita Thrust Front compressed the region. The Lampasas arch extends northeast from the Llano uplift, striking parallel to the thrust front.

The effects of the Ouachita Orogeny weren't purely structural. The formation of the Ouachita Thrust Front Mountains and the adjacent Fort Worth Basin led to shifts in deposition and constraints upon depositional patterns.

The early Pennsylvanian Morrowan age Marble Falls Limestone was deposited atop the Barnett Shale. The Marble Falls is a non-porous layer that acts as an excellent fracture barrier. The deposition occurred as the region was inundated beneath transgressive seas, which are more indicative of renewed basin subsidence than global eustasy changes. On well logs, the layer presents a thick, almost 600 ft in many places, very clean limestone, with little clay. Even with the poor porosity, the Marble Falls is targeted as an unconventional reservoir as oil and gas migrated upward from the Barnett Shale to become trapped in the pore-spaces (Loucks et al., 2004). With the Ouachita Orogeny creating a compressional environment, the region underwent subtle folding as the layer deposited, causing there to be slightly thicker accumulations in synclinal regions and thinner accumulations in anticlinal ones (Johnson et al., 1989). Near the base of the Marble Falls, there is a thin 50 ft shale layer that is below the seismic vertical resolution and is often mistaken on well logs for the Barnett, and thus is called the "false Barnett". The entire limestone sequence thins rapidly to the south, and grades into shale to the west.

Pennsylvanian age rocks above the Marble Falls are largely a mix of fluvial rocks and occasional carbonates. The first major structural movements took place in the Pennsylvanian Atokan time (Hentz et al., 2012). The faults along the sides of the Muenster and Red River Arches were activated and the blocks uplifted, causing them to become sediment sources for the subsiding basin. Besides rejuvenating old basement faults, the tectonic activity caused the creation of new faults in the northeastern part of the basin striking parallel to sub-parallel to the older Mineral Wells Fault. With the Ouachita Front compressing the entire area, the basin as a whole began to tilt to the west, progressively shifting deposition centers in a westerly direction. The formation of the Bend Arch was a combination of the basin formation on the east and the westward tilting forming the western limb. The Atokan age depositional shift caused the progradation of fluvial systems into the basin. The layers deposited during the Atokan are called the Bend

Group and consist mainly of westward prograding fluvial systems and some intermittent transgressive carbonates. The conglomerates that make up the Bend Group are largely sourced from the uplifted arches and the Ouachita Thrust Front filling down into the basin as it subsided and the center of deposition shifted westward. Since the faulting was contemporaneous with deposition, movement of vertical fault blocks acted as a constraint for deposition. Within the northeastern portion of the basin, deposition of the Pennsylvanian Atokan age Bend Conglomerate is theorized to have been guided by the M ineral Wells Fault System running through the area. Despite the high level of tectonic activity, dips within the layer are no more than three degrees (AlHakeem et al., 2013).

The lower Atokan is characterized by mix of fluvial compositions, while the upper Bend group becomes increasingly marine. The lower Atokan conglomerates have a largely digitate form, with long channel banks reaching far out into the basin resembling a hand with fingers widespread. The conglomerate, shale and sand of the Lower Atokan grade into one another, with no clean sand, shale or limestone layers thicker than the seismic resolution. The jumbled nature of the sediment leads to the Bend Group being seismically incoherent with intermittent channels and deltas (Johnson et al., 1989). Many fields throughout the basin produce from this conglomerate reservoir, with gas sourced from the Barnett Shale. The areas of adequate porosity are discontinuous and thin, corresponding to the shifting, prograding and transgressing fluvial systems (Hentz et al., 2012).

Above the jumbled conglomerates lies a regionally extensive clean lime termed the Caddo Limestone. Seismically, the Caddo Limestone presents a clear and unbroken reflector, making it excellent for seismic well ties. The Caddo Limestone is the lower unit of the Strawn Group, which was deposited in the Pennsylvanian Desmoinsian and lies conformably atop the Bend Conglomerates. In some regions, very clean Caddo Limeston e is very thick, but in the northeastern portion of the basin its thickness is closer to 100 ft. With a porosity ranging from 7 to 14% but low permeability, the Caddo Limestone has been found to sporadically contain gas sourced from the Barnett Shale.

The layers just above the Caddo Limestone are genetically very similar to the deeper rocks of Atokan age. The layers represent a mix of shale, thin limestone beds and sporadic sands within the extensive lobate Perrin Delta Complex that stretched across the northern half of the basin from the shoreline on the east. The layers deposited during the middle Desmoinsian are more closely related to the rocks above them, marking a decrease in the rapid sedimentation rates. During the middle Desmoinsian time there were several cycles of sea level transgression, resulting in limestone layers, and regressions, resulting in more fluvial deposits. These quartz sand channels within the Strawn group present high porosity reservoirs, which contain largely brine, but in some places local oil and gas accumulations (Johnson et al., 1989).

The Missourian age Canyon Group reflect the withdrawal of the Epeiric Sea near the end of the Desmoinsian as the thick layer of largely basinal clastic rocks were deposited. While primarily mixed deposits of calcareous sandstones, clays and shale, the group is also marked by intermittent limestone layers. This is characteristic of the cycles the basin underwent as the Perrin Delta Complex continued to ferry sediment from the Ouachita front into the basin, with the highly constructive deltas prograding atop the older rocks. Periods of marine encroachment resulted in the buildup of carbonate shelves atop abandoned delta lobes, which in turn were sufficient to deflect the continued progradation of the Perrin Delta Complex (Johnson et al., 1989).

The end of the Pennsylvanian is marked by the accumulation of the Virgilian age Cicso Group, a succession of rocks very similar to the underlying strata. Dominantly comprised of clay and shale, there also exist intermittent sandstones and repetitive beds of limestone around 10 ft thick. Due to the exposure of the eastern basin edge by the compressive Ouachita Front, Cicso Group rocks are limited in extent to the very northern and western part of the basin.

At the beginning of the Permian, the region became elevated above sea level creating an unconformity between the Permian strata and the underlying rocks. Burial history reconstructions suggest that a thick section of Pennsylvanian and early Permian rocks totaling an estimated 4000 ft has been eroded. Tectonic activity paused in the Permian and the sedimentary layers were deposited in a tectonically quiet environment as the basin subsidence continued. Despite the lack of tectonic activity from the Ouachita Orogeny, the Mineral Wells Fault continued to undergo periodic reactivation. With the cessation of compression from the Ouachita Thrust Front, the westward tilting ceased. Due to the shape of the basin, and the previous westward tilting, layers of Permian age were deposited in the northwestern part of the basin (Pollastro et al. 2007). Permian age sands contain sporadic oil and gas accumulations, and represent the shallowest conventional reservoir rocks in the stratigraphic column. As the Ouachita Orogeny ended, the mountains were left to the elements and by the middle Permian had eroded down to low hills.

Subsidence and deposition in the Fort Worth Basin ended in the Permian as the region became a dry inland region. There are no Triassic or Jurassic age formations in the northeastern portion of the basin as well, but the time period was far from quiet. Within the basin the compressional environment that had existed during the Pennsylvanian shifted to one characterized by extension. Rifting began along zones of weakness within Pangaea during the Triassic, eventually breaking up the super-continent and forming the Gulf of Mexico and the Atlantic Ocean. The beginning of the Jurassic saw the opening of the Gulf of Mexico along the southern plate boundary as the convergent boundary changed and began ocean spreading. These zones of weakness opened along the eastern portion of what would become the United States, and in the Middle Jurassic the Northern Atlantic Ocean was created (Montgomery et al. 2005).

Tectonic activity shifted west as the North American continent underwent continued tectonic stress with the thin-skinned deformation of the Cretaceous age Sevier Orogeny and the thick-skinned deformation of the Paleogene age Laramide occurring in the west. Despite the region being located inland, an inland seaway stretched downward from the north during the middle to late Cretaceous, once again placing the region within an epeiric sea way. As the Gulf Coast was a passive margin, the rocks deposited within the Cretaceous seaway are largely devoid of deformation with only a slight amount of folding. The thin veneer of Cretaceous rocks are devoid of oil and gas, but the porous conglomerate is home to many major aquifers. These rocks are overlain by modern alluvium and river terrace deposits.

Very recently geologically, the Balcones Fault system was formed along zones of weakness in the Ouachita Thrust Belt, a result of subsidence along the Gulf Coast from sediment loading. This Miocene extension led to the creation and reactivation of numerous normal faults and grabens.

Chapter 3: Surrounding Oil Fields

The Fort Worth Basin is home to many oil fields, both conventional and unconventional. These hydrocarbons are all sourced from the Barnett Shale, with gas occurring in the deep eastern portion of the basin against the structure of the Ouachita Thrust front and changing phase to oil as the basin shallowed up over the Bend Arch. Many of the wells target shallow conventional targets, but the larger number of productive wells are unconventional wells targeting the gas producing northeastern portion.

The Barnett Shale was deposited during the Mississippian with an average 4% TOC, richer in the south. For a clastic rock, even given absorption and adsorption, 4% TOC is a very rich source rock. Conventional reservoirs range throughout the basin, and consist of channel sands, thick conglomerate, and porous limestone. The shale layers that occur intermittently amongst the sands, conglomerates and limestone layers provide seals for these reservoirs. As the basin subsided, the Barnett Shale reached thermal maturity in the early Permian, producing gas in the deeper northeastern part of the basin.

3.1: Newark East Field

Located just west of the city of Fort Worth in Jack and Wise Counties, the Newark East Gas Field was the largest gas producing gas field in Texas during 2006. Discovered in 1981 by Mitchell Energy, the Barnett Shale was the first major source of shale gas in the United States.

The field has been divided into the core region, where the Barnett Shale sits directly atop the Viola Limestone, and the expansion area, where the Barnett sits atop the

Ellenburger Limestone (Martineau et al., 2007). After Devon bought Mitchell, they drilled several experimental horizontal wells into the Barnett and were met with so much success that it spurred a shift from vertical to horizontal drilling. The number of wells producing in the area has increased exponentially since the early 1980s. As of 2006, the field had produced 2.3 trillion cubic feet of gas and was producing 2.0 billion cubic feet per day.

The main risk within the Newark East Field are faults and fractures acting as conduits for water from the Ellenburger Limestone. Gas is stored within the Barnett Shale in pore spaces, natural fractures and gas that is absorbed into the clay (Martineau et al. 2007). There are larger fractures that are due to karsting within the underlying Ellenburger. These karst features cause round collapses within the Barnett, and the large scale fractures in the highly karsted regions allows the escape of stored gas by fracturing upward through the Marble Falls Limestone (Martineau et al., 2007). The fracturing also prevents the continuous accumulation of additional gas. In addition to karsting in the Ellenburger, the region is also characterized by larger faults, most notably the Mineral Wells Fault, which runs NE to SW perpendicular to the Muenster Arch. It has a component of left-lateral strike slip motion and is downthrown to the north into the deeper portion of the basin. The Mineral Wells Fault is the largest fault through the area, but it is just the largest component of the Mineral Wells-Newark East Fault system. There are many smaller component faults in the area that strike parallel to sub-parallel to the major fault. There are also localized folds that occur along the northeastern portion of the fault along the Muenster Arch.

Due to the drop in productivity around karsted and faulted regions, many seismic surveys have been collected in the region to better plan wells. Most of these surveys are from the core area of the field, meaning that major faults in the region are well mapped. All of these surveys reveal subtle folds and fractures in the flat lying shale bed.

Current estimates show that there is still a large amount of gas to be recovered in the area. Future expansion of the field will continue as gas prices rise again.

3.2: Ranger Field

Ranger Oil Field is located in Eastland County, and was one of the most productive US oil fields discovered in the early years of Fort Worth Basin exploration (Reeves et al., 1922). It is a fairly small field in comparison to the Newark East Field, with only a couple hundred wells instead of thousands. Despite being such an old field, it is similar enough to the study area in geometry and structure to be considered an analog.

Before 1917, only sporadic shallow wells had been drilled in the area, targeting shallow sand channels. Once they started drilling deeper, they found a pair of very productive layers, a hot shale and black limestone layer. These drilling efforts marked the first discovery of the Mississippian age Barnett Shale and the overlying Marble Falls Limestone. Most of the oil in the field is sourced from the Marble Falls Limestone.

Structurally, the field has very low dips, and the layers are fairly flat. The larger structure that traps the oil within the field is a gentle monocline striking to the northeast and dipping off to the northwest. There are also faults within the field. These faults strike NW-SE, and are largely normal with vertical displacement.

3.3: Boonsville Field

The Boonsville Field is spatially in the same area as the Newark East Gas Field, but produces from a much shallower reservoir. It is roughly 2,300 square miles encompassing both Jack and Wise Counties, making it the largest field producing from the Atokan age rocks. Originally drilled by Mitchell Energy, production from the field has been on the decline for the last 30 years (AlHakeem et al., 2013).

Gas within the Atokan age Bend Conglomerates was discovered in the 1950s. The gas produced is sourced from the Barnett Shale, but migrates upward through the faults of the Mineral Wells Fault System and fractures caused by the karst collapses within the older Ellenburger Limestone. The reservoir within the field is the porous and permeable Bend Conglomerate, which was deposited off the coast of the Ouachita Thrust Front Mountains into the epeiric sea that covered most of the basin as a complex system of alluvial fans and channels. Due to the nature of the deposition of these conglomerates, reservoir quality varies both laterally and vertically, leading to multiple zones of pay within the Atokan age Bend Conglomerates bounded by shale layers.

Structurally, there are numerous faults within Boonesville field, many associated with the Mineral Wells Fault System. These faults are largely high angle normal faults that are downthrown to the north. The combination of fault scarps and karst collapses causes local highs and lows that look a lot like anticlines.

Basin-wide, as of 2011, fields producing from the lower Atokan reservoirs had produced more than 3.2 Tcf of natural gas and more than 36.3 billion barrels of oil.

Chapter 4: Seismic Volume

The seismic survey examined in this thesis is located in the northeastern part of the Fort Worth Basin near the southwestern corner of Wise County (Figure 5). The main survey was acquired in 1999 and covers around 125 square miles. The main survey was then merged with two older surveys. The older of them, acquired in 1995, was a fairly small survey located in the center western half of the merged survey. It was acquired with both short offset and narrow azimuth, leading to poor data quality. The other survey, just to the south, was collected in 1997 with long offset, but still narrow azimuth data, meaning that the data quality was better, but still with noticeable noise. The main survey was acquired with long offset and wide azimuth, so the data quality is much improved. The merged survey has areas of noticeable noise that delineates the two older surveys (Figure 6). In 2013, a University of Oklahoma Masters Student Alfredo Fernandez reprocessed the survey in order to improve resolution and remove migration artifacts present in the original survey. His thesis re-migrated the data in order to “better image the Mississippian and Ordovician targets” to improve “seismic attribute characterization of the internal architecture within the Ellenburger Group karst-collapse features” (Fernandez et al., 2013). Remigration was necessary because the original data had rampant migration errors within the basement directly underlying the Ellenburger Limestone (Figure 7).

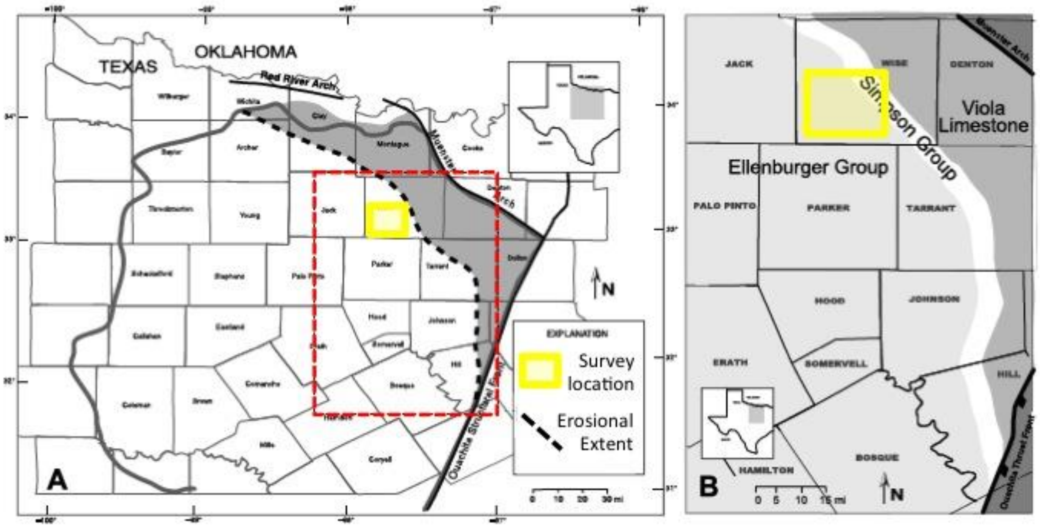

Figure 5. Map of the Fort Worth Basin showing the eroded extent of the Viola Limestone. On the western half of the survey the Viola Limestone has been eroded. The presence of the Viola Limestone on the east indicates that area wasn't subaerially exposed and eroded in the late Ordovician. From Pollastro et al. (2007).

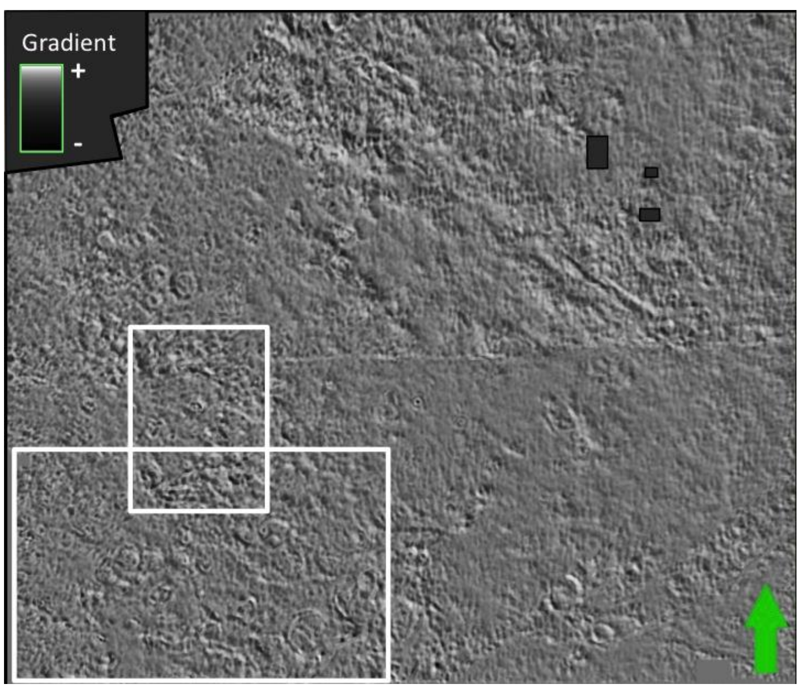

Figure 6. Map of overlain inline and crossline energy gradient showing the increase in noise in the two older surveys. The two older surveys were acquired in 1997 and 1995, with narrow azimuth acquisition. This time slice is at 1.19s through the overlain inline and crossline energy gradient volumes.

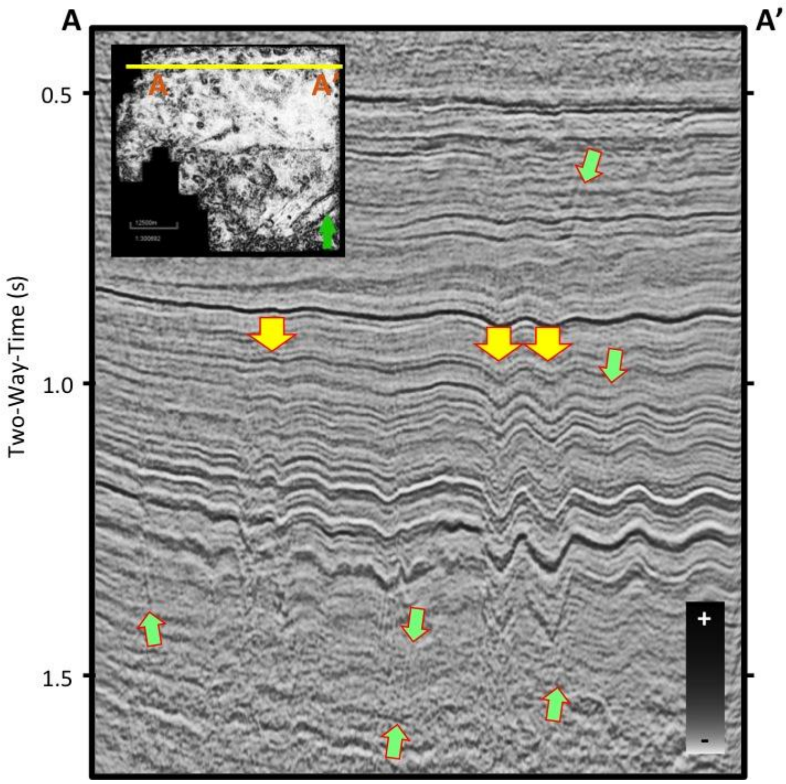

Figure 7. Seismic line AA' showing migration errors within the basement, and diffractions from high angle edges of the karst collapses. The yellow arrows indicate karst collapse, while the green arrows indicate migration noise.

The earth filters all wavelet data to minimum phase, but the data was processed to use a zero-phase Ricker wavelet. The survey has good frequency range data, between 8 and 125 Hz and was collected targeting the Barnett Shale at an average depth of 6700 ft, or 1.1 s two-way-time, within the survey. The dominant frequency at Barnett Shale depth is 40 Hz, with an interval velocity of 12000 ft/s (3658 m/s). The sample interval was every 2 ms, which is more than enough to accurately represent the seismic signal at the Barnett Shale depth, sampling the data 12.5 times every cycle. The dominant wavelength at the Barnett Shale depth is 300 ft, meaning that the tuning thickness is around 75 ft. Any layers below the tuning thickness will decrease in amplitude and be essentially averaged into the layers around it, meaning that only thick layers or packages of rock would present clear, consistent reflectors. Layers that are thick enough to present clear reflectors within the survey are the deep Ellenburger Limestone, Barnett Shale, Marble Falls Limestone and shallow Caddo Limestone.

The main seismic survey was acquired with a receiver spacing of 220 ft and a receiver line spacing of 880 ft. The shots were spaced 220 ft apart, with 5 pound shots drilled to 60 to 80 ft deep. There were 12 live receiver lines per shot with 71 active geophones each. The CMP bin size was 110 ft by 110 ft. The maximum CMP fold is 49 in the interior of the survey and the average fold is 26 (Figure 8). Despite stacking to attenuate ground roll and coherent noise, the ground roll remains a strong 20 Hz signal, overprinting the near offset seismic signal. The frequencies between 10 and 100 Hz imaged geology, with higher frequencies largely representing noise (Fernandez et al., 2013).

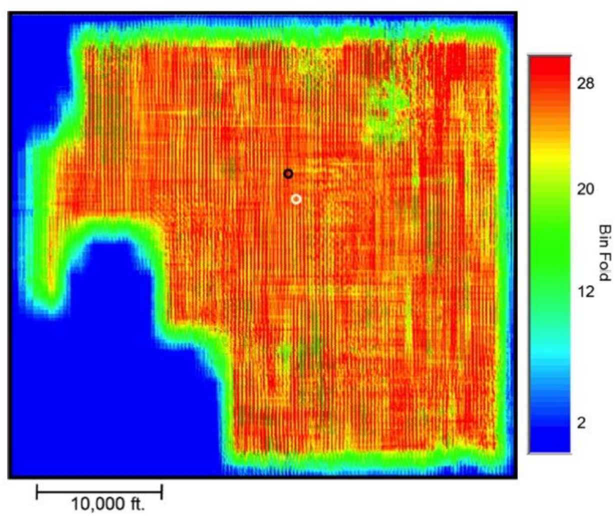

Figure 8. Figure showing the fold across the reprocessed survey. The average fold within the survey (excluding the two older surveys) is 26. Predictably, fold is higher in the center of the survey. From Fernandez et al. (2013).

Chapter 5: Previous Geophysical Work

Much previous work has been completed focusing on the Barnett Shale and Ellenburger Limestone within the dataset. The academic work ranges from simple interpretation of karst collapse features and their effect on the Barnett Shale production to the more difficult task of trying to tie karst collapses to basement faulting.

Sullivan et al. (2006) published the earliest academic analysis of the dataset, using seismic attributes to understand the origins of karsting and collapse chimneys. They hypothesize that the collapse karst chimneys occur due to faulting in the basement creating weak spots in the overlying carbonates. The Ellenburger Limestone is a complex layer characterized by mature cockpit karst topography. Areas with low porosity remained while other areas underwent dissolution and the formation of pre-burial cave systems. Sullivan et al. (2006) posit that the collapse chimneys, while overprinted with the signature of some subaerial karsting, were first-order controlled by "bottoms-up tectonic induced extensional collapse." Small fractures were widened by dissolution into caves that eventually collapsed. The evidence of subaerial exposure comes in the form of channels atop the Ellenburger that were identified using the energy gradient in both directions. In Figure 9 yellow arrows outline collapse features, purple lineaments indicate faults and the green arrows possible channels atop the Ellenburger. The presence of channels indicate that after the Ellenburger deposition, subaerially exposure occurred and the channels were down-cut. In the region of this survey, the Upper Ordovician age Viola Limestone has eroded away, a result of the subaerial exposure (Sullivan et al., 2006).

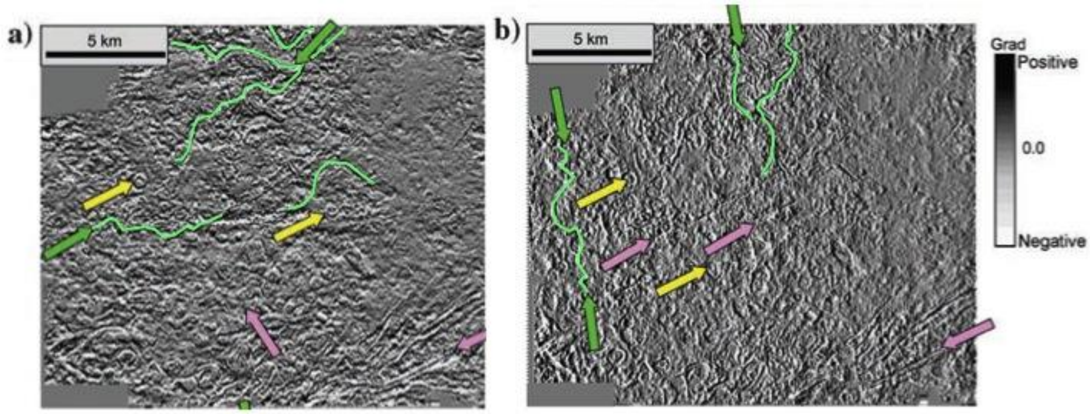

Figure 9. Figure from Sullivan et al. (2006) Showing the inline (a) and crossline (b) energy gradient highlighting channels and lineations atop the Ellenburger Limestone at TWT=1.19 s. From Sullivan et al. (2006)

Sullivan et al. (2006) theorize that the karsts are due to a system of faults that extend upward from the acoustic basement (Figure 10). They interpret close to twenty faults, some of them extending as far upward as the Caddo Limestone. The faulting in the basement is controlled by stress in the region, so regional strain regimes were analyzed at multiple layers. The strain at the Ellenburger Limestone level has the main component E-W with smaller components NW-SE and NE-SW. At the shallower Caddo Limestone level, the primary stress direction had shifted to NW-SE with only minor components E-W. At the surface, the stress regime is extensional, a reversal from the Ouachita Compressional environment during the Pennsylvanian. These strain orienting “rose diagrams” are invaluable when examining the faults and lineations within the seismic data.

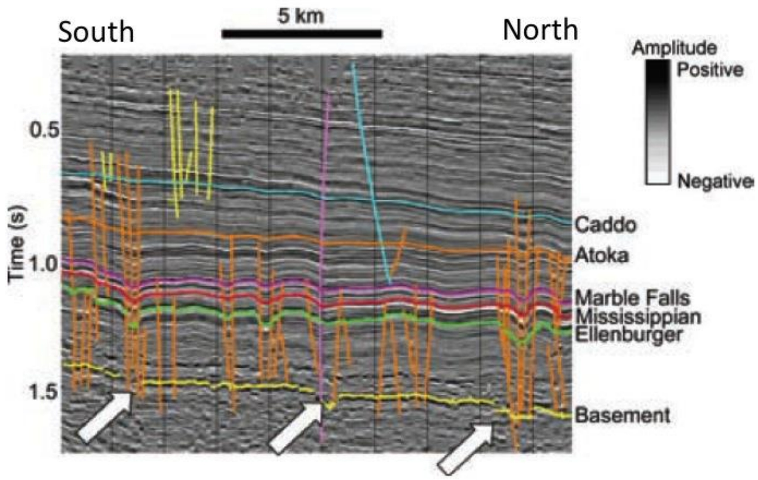

Figure 10. Sullivan et al.'s (2006) interpretation of the continuation of sedimentary faulting and karst collapses into the basement. Basement involved faults are in orange, and faults that aren't basement involved are in yellow.

Elebiju et al. (2009) used gravity surveys to identify of basement faulting. Using pre-stack time migrated data and high resolution aeromagnetic data, his goal was to correlate sedimentary faulting and karst collapses to basement features. The fractures in the sedimentary section trend sub-parallel to the Muenster Arch, but the basement is highly incoherent, making even the largest faults indistinguishable from the surrounding noise.

Gravity lineaments that link basement faults and the sedimentary faults visible in the seismic section. High-resolution aeromagnetic data (HRAM) is also effective in mapping Precambrian basement faults.

The map of the horizontal gradient magnitude, as well as the Euler deconvolution plot (Figure 11) show a gravity high that runs NE-SW across the lower right corner of the survey. Seismic attributes were utilized to examine the faulting along the layer.

Examining coherence, a measure of the similarity between neighboring traces, revealed two main fault systems within the survey. The arrows marked with F1, F2 and F3 are indicating faults within the survey. To look at gravity data, both residual gravity and Euler Deconvolution were examined. The residual gravity is the signal that remains after the larger variations, such as those on a continental or mantle scale that represents the basement lineaments in the area. The Euler Deconvolution is a popular tool for quick initial interpretation since it is simple to calculate and interpret. It examines the x, y, and z location of data points in combination with the structural index. The wrench fault in the southeast has a gravity high, which suggests that the fault system in the sedimentary sequence has roots deep in the basement. A lineation appears on the Euler Deconvolution parallel to, and just north of the graben, suggesting that the fault plan may dip in the basement toward the northwest. The large fault labeled F1 is identified as an antithetic strike slip fault, and is not visible on the gravity maps. The inability of the fault to be imaged implied that the fault was not significantly offset enough to perturb the gravity readings. Elebiju et al. state that another possibility if that the fault curves to the northwest at depth, causing some of the anomalies further to the northwest. There are multiple gravity anomalies throughout the survey though, and many of these lineaments don’t correspond to any faults visible in the seismic. The anomalies don’t correspond to the NE-NW oriented karst collapse lineaments either. They may represent some of the highly curved and discontinuous intra-basement reflectors that may represent igneous intrusions.

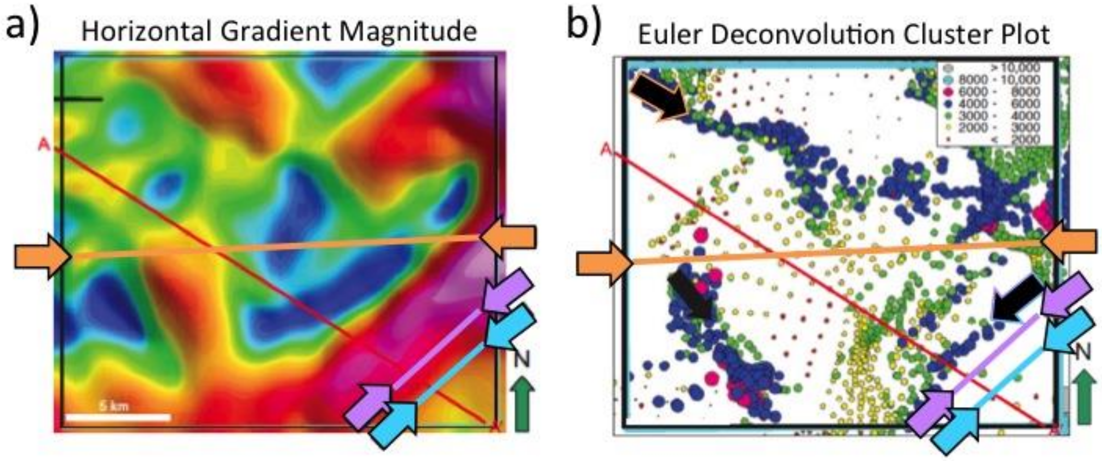

Figure 11. Gravity data showing (a) horizontal gradient magnitude and (b) Euler deconvolution cluster plot. Gravity anomalies such as this can indicate the presence of basement faulting. Note the high gravity anomaly in the southeastern corner in (a), perhaps corresponding to the graben feature. On the right, note the lineation that parallels the graben feature.

The study concluded that there was both evidence for and against the sedimentary faults being basement controlled. The wrench fault aligns with a gravity lineament to the northwest, suggesting the fault plane is dipping to the northwest at the basement level. The strike slip fault through the center shows no gravity anomaly, despite the fault dropping down on the northern side. Based on his conclusions, he felt that the HRAM lineaments could be used to predict basement involved graben features.

In 2013, the data was reprocessed in order to remove migration artifacts from originally using the wrong migration velocities at depth. Fernandez at al. (2013) reprocessed the data, and then wrote a thesis to examine the deep Ellenburger Limestone. The Ellenburger karsting posses a drilling risk where the fractures act as conduits for water to invade upward.

Karst collapses are strongest at the Ellenburger Limestone level where the collapses began. The decrease in amplitude upward indicates that the collapse was episodic and decreasing in magnitude by Pennsylvanian Atokan time. He also suggests that the collapsing may have instead been reactivated. By the Caddo time, the collapses cause no discontinuities, just minor curvature anomalies due to differential compaction. The faults within the survey are briefly mentioned, and he theorizes that the large E-W strike slip fault that runs through the survey is one of the faults making up the Mineral Wells fault system. After much work with the velocity field, the reprocessed data cleared up the migration artifacts within the Ellenburger Limestone. As part of his processing, however, Fernandez cut out portions of the two higher noise older data sets. This reprocessed seismic survey is the one used for much of the attribute work, given the survey's improvement in noise interference from the original merged dataset.

Many studies have focused on other portions of the Fort Worth Basin as well. In his 2010 paper Elebiju et al. examined an additional survey from within the basin. This additional survey was characterized by both faulting and karsting, consistent with the survey in this paper, however these faults weren't parallel to the Mineral Wells Fault system. The features within the additional survey primarily align along NW-SE and NE-SW lineaments. The results of this study were inconclusive as well, finding that the gravity both aligned with and occurred unrelated to the sedimentary faulting.

The same year, Olubunmi O. Elebiju partnered with Elizabeth Baruch and Roderick Perez to analyze two other seismic sets along the Mineral Wells Fault system. These were located to the east of Wise County in Denton County and just south in Parker County. The northeastern survey has two large faults that are part of the Mineral Wells fault system. Both surveys have abundant faulting, but the karsting in the surveys supports Sullivan et al.'s earlier conclusion that areas with the Viola Limestone are less heavily karsted (Figure 5).

Just to the east of the survey, a thesis by Melia Rodriguez examined the correlation between 3D seismic attributes in the Barnett Shale and production in eastern Wise County. The correlation to production is achieved by examining the faulting and karsting within the survey. Fracturing within the shale would release the gas from the layer and result in poorer production. More brittle areas are dominated by quartz, less ductile and easier to hydraulically fracture. They found that the combination of brittleness index maps and curvature maps accurately mapped areas within the Barnett Shale that had higher productivity.

With the same data, Suat Aktepe of the University of Houston analyzed the difference between time migrated data and depth migrated data for imaging the basement. In this study area, karsting is all but absent, leading to the basement reflector being unbroken and therefore much easier to image. These basement rocks are high velocity Precambrian granodiorites and metasediments, but are usually broken, poorly migrated and obscured by the high amplitude reflector of the high velocity Ellenburger Limestone. The depth migrated data creates more exaggerated topography in the upper layers, but especially in the basement, where a high patch corresponds to the upthrown side of the fault in shallower layers. This depth migration of the data suggests basement involvement of the two major faults within the system.

All of these studies focused on the faulting, karsting, and production within the basement, Ellenburger Limestone, and Barnett Shale respectively. This focus on the deeper layers neglects the wealth of information present within the shallower layers. Few, if any papers mention the Pennsylvanian age layers that record the progression of the Ouachita Orogeny and subsequent deformation.

The Marble Falls Limestone is occasionally examined in its capacity as an unconventional reservoir holding gas and oil from Barnett Shale. The Marble Falls marks the last layer deposited before the main portion of Ouachita structural deformation began at the end of the Pennsylvanian Morrowan time. After Pennsylvanian Morrowan time, the greater structural deformation within the basin became extremely important to the geometry of layer deposition. Examining the structural and stratigraphic features of post Mississippian layers within the survey will provide insight into the changes within the Northeastern portion of the basin.

Chapter 6: Interpretation of the Time Migrated Volume

The structural and stratigraphic characteristics of the layers within the survey were examined by looking at attributes. These maps examined different aspects of the data to highlight certain features.

Several layers were coherent enough for the construction of two-way-time maps. Despite being heavily karsted, the Ellenburger Limestone, Barnett Shale and Marble Falls Limestone were coherent enough to image. Shallower, the Caddo Limestone presented a strong reflector that remained unbroken by the karst collapses.

Faults and karsts are best represented by coherence maps (Figure 12). These maps highlight edges within the seismic data, whether it is the edge of a karst collapse, channel or fault plane. Highlighting edges is done by computing the amount of similarity between neighboring traces, with a value of one indicating that the neighboring traces are perfectly similar and a value of zero meaning that the neighboring traces are completely different. Several different types of coherence were computed, with the clearest being the Sobel Filter Similarity, which computes a magnitude of the derivative of the amplitude along local dip and azimuth.

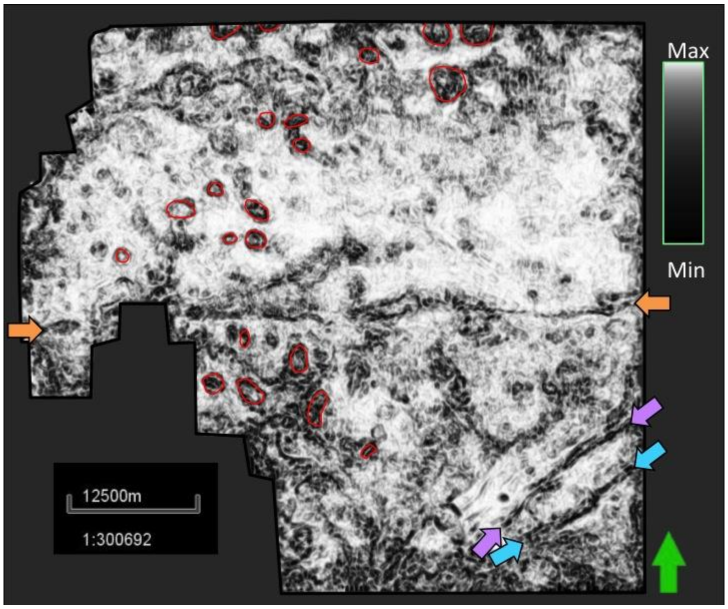

Figure 12. Time slice at t=1.19 s depth through the Sobel Filter Similarity volume. Note the faults, shown in orange, blue and purple within the survey. Karst collapses are rimmed in red. These karsts are the most prevalent on the western half, and most incoherent in the southwest.

Figure 13 shows the most positive and the most negative curvature. Domes and ridges have a high K1 value and are red on a K1 map. On a map of K2, the most negative value of a dome would still be positive and would appear a weak red on that map as well. In contrast, a saddle, would have both a strong red K1 and strong blue K2 value. Ridges would appear as red lineations on K1 and valleys would appear as long blue lineations on K2 maps. Karsts would be blue circles surrounded by red rings. The curvature maps are most useful when the K1 and K2 are overlain to see the interaction of strongly positive and strongly negative events. Curvature can be used to look at very large channels, karst collapses, grabens, horsts, and faults where there is drag on the fault plane.

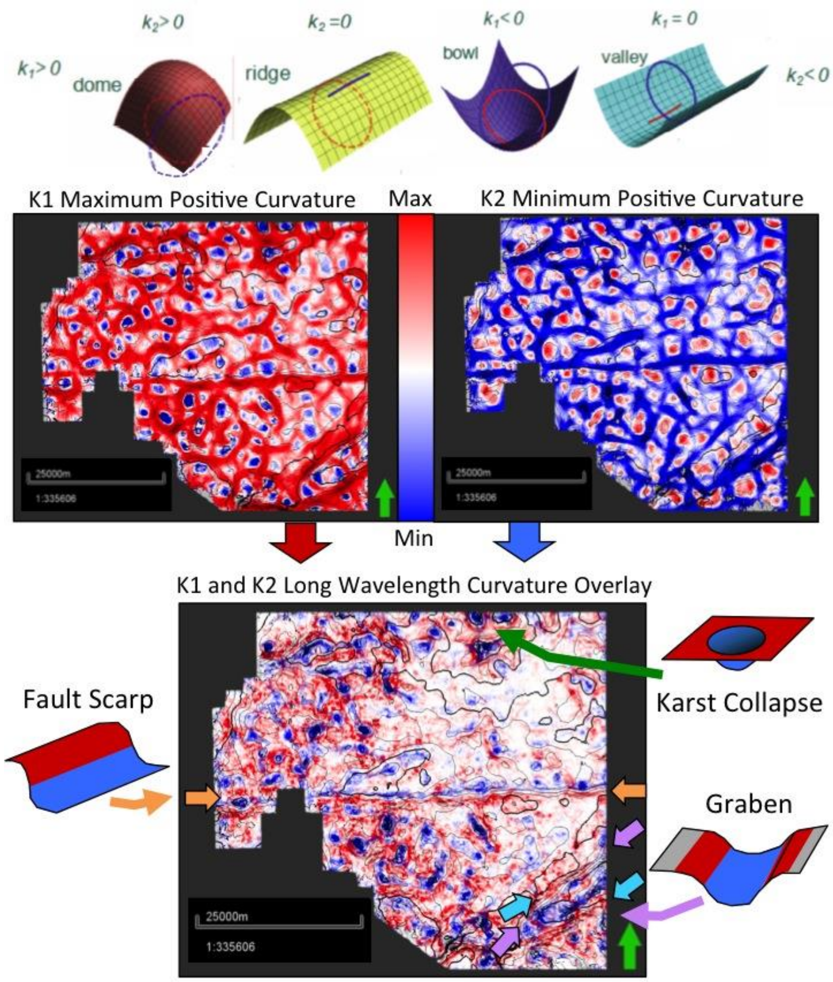

Figure 13. Explanation of the curvature attribute showing the time slice atop the Marble Falls Limestone. When the K1 most positive curvature (top left) is overlain with the K2 most negative curvature (top right) red features represent ridges and domes and blue features represent valleys and bowls. Shape index from Fernandez et al. (2013).

A related attribute is the shape index, which combines the K1 and K2 curvature to map bowls, valleys, saddles, ridges or domes. A shape index map can be seen in Figure 14 with the darkest blue indents representing karst collapses.

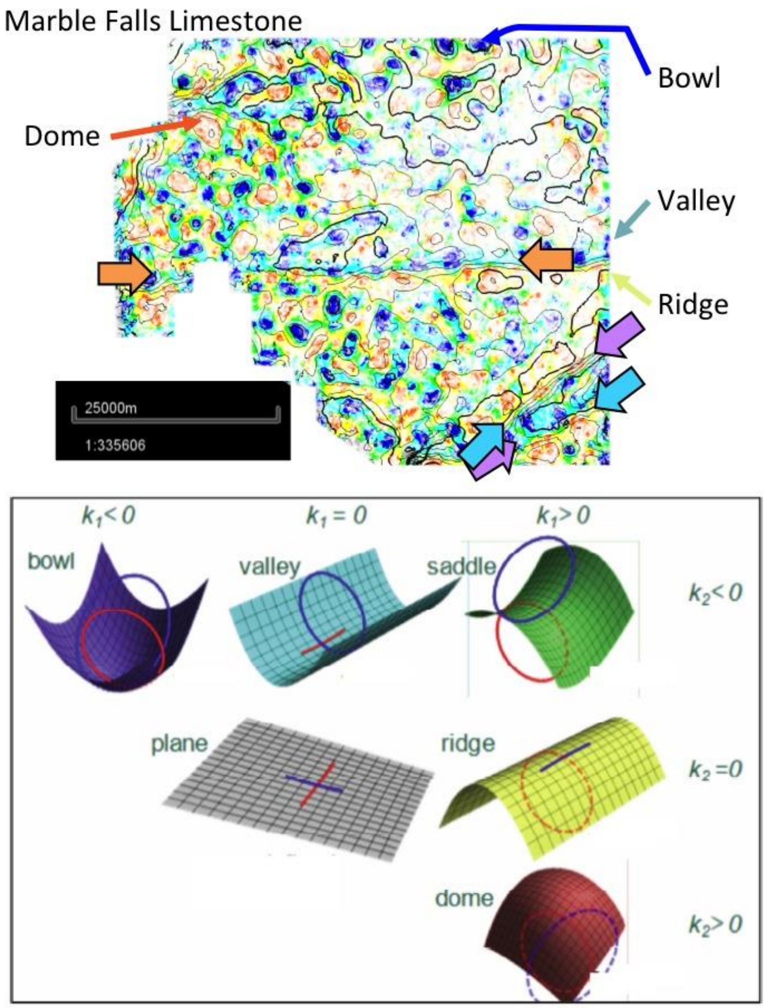

Figure 14. Explanation of shape index maps. These maps are constructed using a combination of K1 and K2 in order to color code bowls, valleys, saddles, ridges, and domes. From Fernandez et al. (2013)

Another helpful attribute is the co-rendered dip azimuth and dip magnitude, useful in showing the dip direction of fault scarps, and the edges of grabens and horsts (Figure 48).

Energy gradient maps are constructed from the horizontal derivatives of coherent energy along structure in the inline and crossline direction. The two different directions of gradient are helpful in visualizing directional thin features, like slumps or channel edges (Figure 9). Another attribute that can sometimes be helpful in delineating channels is RMS amplitude. The root-mean-square amplitude computes the square root of the sum of squared amplitudes divided by the number of samples within the specified sample window. The RMS amplitude highlights high amplitude areas, which inside a channel might be an indicator of gas fill (figure 43).

Isochron maps were also a vital tool in the interpretation of basin event timing. These maps are constructed between surfaces in the seismic and show the thickening or thinning of a given layer. These maps can reveal the timing of faulting, karsting and depositional trends (figure 28, 29, 30, 31).

6.1 Well Log Data

Two wells had well logs that ran deep enough to catalog the top of the Ellenburger Limestone (Figure 15) providing a time to depth chart (Figure 16).

Overall the character of the well logs is representative of a fairly mixed lithology, with the only clean, easily correlated formations being the Caddo Limestone, Marble Falls Limestone, Barnett Shale and Ellenburger Limestone.

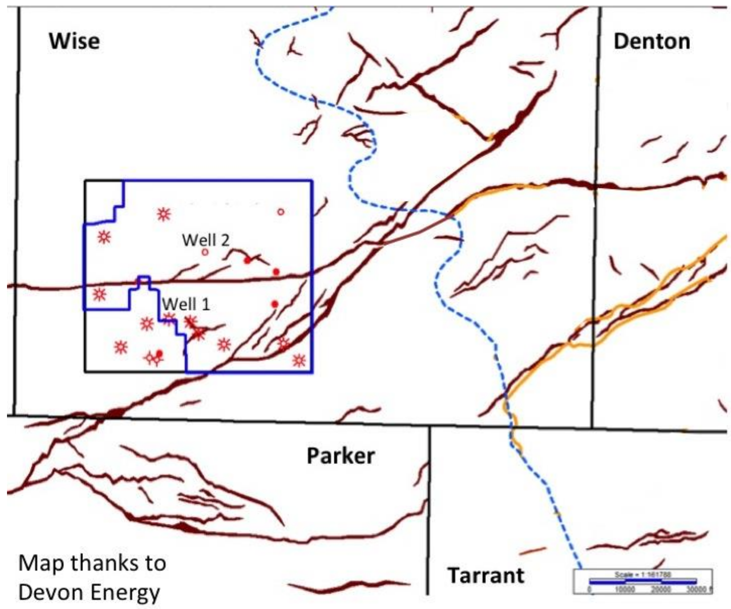

Figure 15. Map showing the faults through the immediate area of the survey. The locations of well 1 and well 2 are marked. Map thanks to Devon Energy.

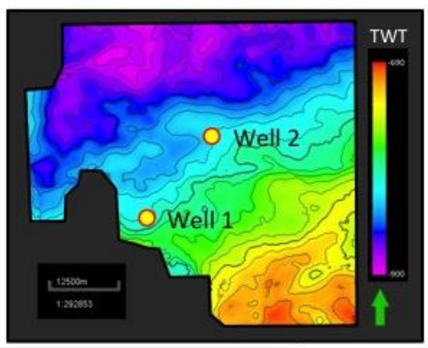

Well Number	1			2		
	Drilled Depth	Subsea Depth	TWT	Drilled Depth	Subsea Depth	TWT
Caddo Limestone	4016 ft	3146 ft	0.8 s	4364 ft	3489 ft	0.82 s
Marble Falls Limestone	6116 ft	5246 ft	1.17 s	6294 ft	5419 ft	1.15 s
Barnett Shale	6510 ft	5640 ft	1.2 s	6761 ft	5886 ft	1.185 s
Ellenburger Limestone	6905 ft	6035 ft	1.245 s	7176 ft	6301 ft	1.25 s

Figure 16. Time-depth conversion chart comparing the sub-sea depths with two-way-time reflections of

major reflectors within the survey. Well data thanks to Devon Energy.

The top of the survey catalogs the Desmoinsian age Strawn group, which is a mix of deltaic sediment prograding to the west. Immediately above the Caddo Limestone, the gamma ray log indicates a large amount of shale, with occasional sand formations indicating a shift in the channels atop the Perrin Delta depositing sand in the area (Figure 17) . The well log character of the sand channels is neither blocky, nor fining in either direction. It suggests that the shift of channel deposition across the lower face of the delta was gradual, not by avulsion. The gamma ray log gradually coarsens upward into mostly clean sands that are punctuated by thin interbedded shale, then fines upward into shale deposition again. These formations have some permeability, indicated by the SP log, but poor porosity, as shown by the narrow gap between the shallow resistivity and deep resistivity indicating very little drilling fluid invasion into the formation. These sands are also highly discontinuous between wells, with sand bodies appearing in well 1 disappearing in well 2 and visa versa, further supporting the theory of channels cutting across the delta face with side areas filling in with marine low energy shale.

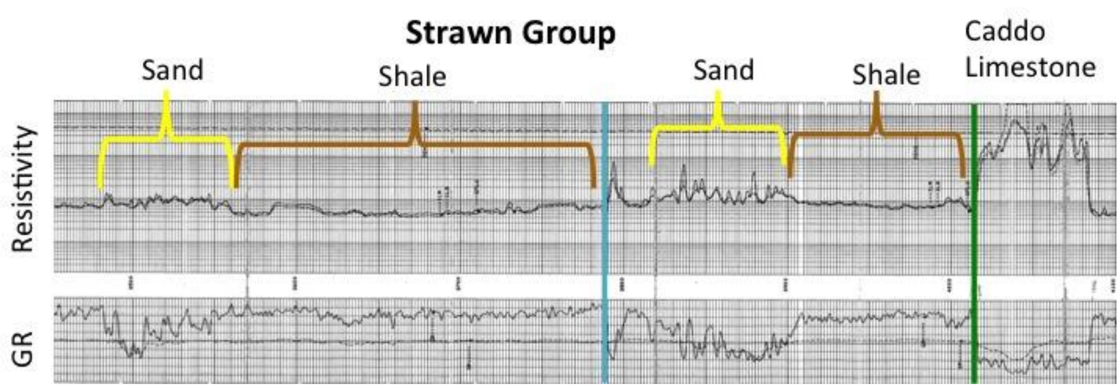

Figure 17. Gamma and Resistivity well logs showing the Upper Strawn Group, with its base in the Caddo Limestone on the right. The formation is largely shale, with silty sands intermittent.

The Lower Desmoinsian Caddo Limestone occurs from around 4000 ft deep in the southern half to 4400 ft deep in the north. Both the top and base of the formation is blocky, marking a very quick transition from shale to clean limestone and back again (Figure 18). Across the survey, the thickness is around 80 ft with very little variation. The formation also has very high resistivity and velocity. Across the logs there is a pronounced dip in the spontaneous potential log that corresponds to a zone of permeability, and additionally porosity as evidenced by the invasion of drilling mud and the gap between the shallow and deep resistivity.

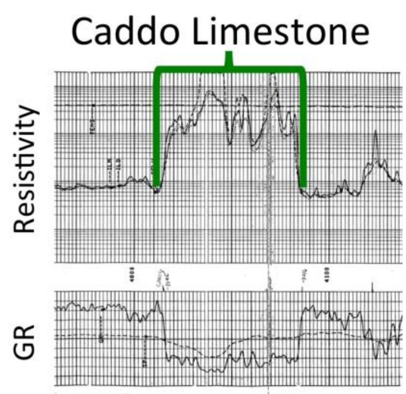

Figure 18. Gamma and Resistivity logs within the Pennsylvanian Desmoinsian Age Caddo Limestone.

Below the Caddo Limestone is the Pennsylvanian Atokan age Bend Conglomerates. Seismically the Bend Conglomerates are jumbled and incoherent, and the well log character explains this. Depositionally, the area was within the Decatur Fan-Delta Lobe complex, composed of course conglomerates. The lithology is a mix or cobbles and silt, with occasional cleaner sands and shale. Porosity and permeability vary wildly within the thick formation. Occasional sandstone channels occur with good permeability and porosity, and are sometimes called the Atoka formation (Figure 19).

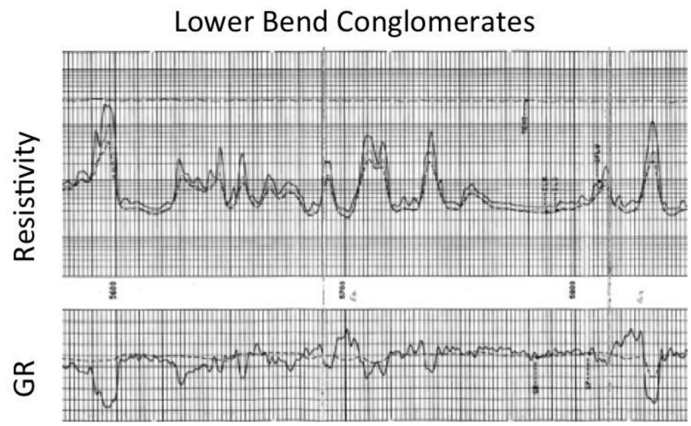

Figure 19. Gamma and Resistivity logs within the Lower Bend Conglomerates, showing the mixed nature of the sediment.

The Marble Falls Limestone lies directly below the Bend Conglomerates. It occurs on average around 6200 ft deep and is around 400 ft thick. It is a very clean limestone, but has low permeability and very little porosity. The low permeability causes it to be an excellent fracture barrier for hydraulic fracturing within the Barnett Shale (Figure 20).

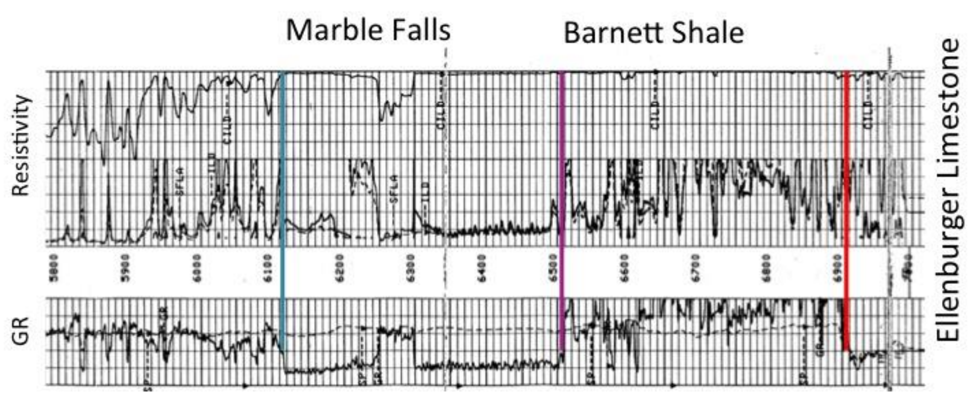

Figure 20. Gamma and Resistivity logs showing the clear horizons of the Marble Falls Limestone, Radioactive Barnett Shale, and Ellenburger Limestone.

The upper Mississippian Barnett Shale is an unconventional target within the basin. It is around 400 ft thick as well, and has regions of shale with very high gamma ray log responses, indicating possible sweet spots.

The lowest layer reached by any of the wells in the area is the Lower Ordovician Ellenburger Limestone. Only the blocky top is visible on the logs taken in the wells. Karst collapses begin at Ellenburger Limestone level.

Within the seismic survey the horizons were correlated to geologic formations using a synthetic seismogram. The bulk density and two-way-travel time from well 1 was used to create a synthetic well tie. These two logs were combined to create a log of acoustic impedance. The differences in acoustic impedance values were used to compute the reflection coefficient at the layer interface. Convolving the reflection coefficients with the wavelet, which was extracted from the seismic data, results in a synthetic seismogram that approximates the seismic data (Figure 21). The seismic signal closest to the well is then compared to the noise-free synthetic seismogram, and geologic well tops from the well logs is correlated to the seismic volume (Figure 22).

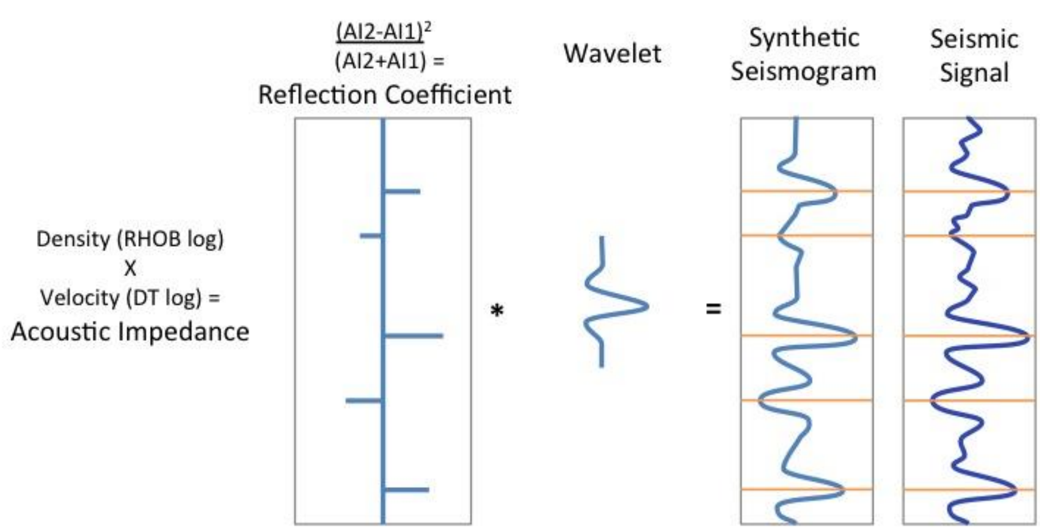

Figure 21. Illustration of the process used to create a synthetic seismogram. The synthetic seismogram is an idealized seismic trace based on the minute shifts in lithology, the seismic signal includes noise.

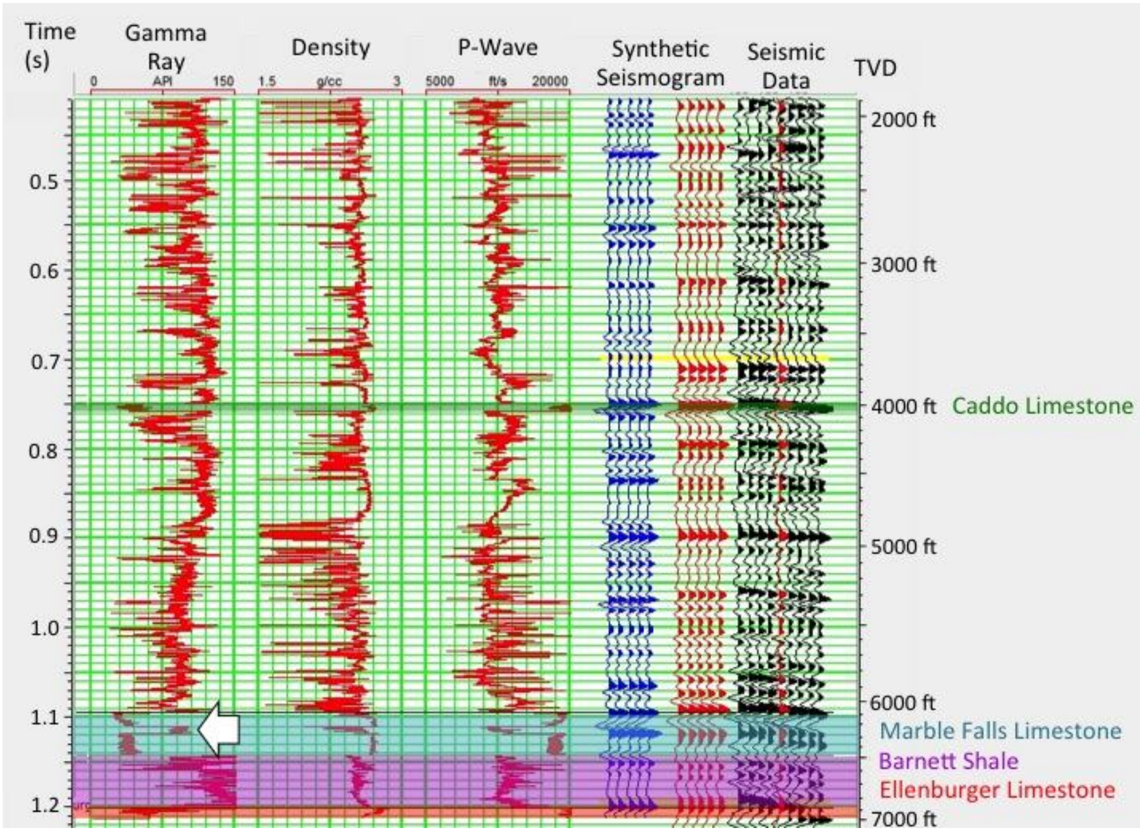

Figure 22. Well tie matching the formations noted in well logs to the seismic data within the survey. Note the strong reflections from all four formations used to tie the seismic. The bright negative reflection within the Ellenburger Limestone marks a shale often termed the “false Barnett”. It is marked by the white arrow. Discrepancies between the synthetic and seismic are due to the difference in resolution: the wells logs record very small changes, versus the seismic resolution at 75 ft.

6.2 Karsting and Stratigraphic Features

The most notable stratigraphic features in the survey are the collapse features. These karst collapses begin within the Ellenburger Limestone and extend upward to the Caddo Limestone. These karsts began as caves within the Ellenburger Limestone when it was subaerially exposed at the end of the Ordovician. These caves were formed by dissolution, and as layers were deposited atop the Ellenburger their weight caused the caves to collapse (Figure 23). On the two-way-time map of the Ellenburger several features can be spotted. The karst collapses are clear, appearing as round aberrations in the overlain coherence image (Figure 24). These karst collapses are heaviest in the western half of the survey supporting Sullivan et al.'s (2006) theory that the karsting was more extensive in areas where the Viola Limestone is eroded, due to longer subaerial exposure leading to more extensive cave systems. The karsts are also visible on the shape index maps. These collapses continue upward through the layers, with the magnitude decreasing by the time that the Caddo Limestone was deposited (Figure 25). The Barnett Shale has less pronounced, yet notable collapses. By the depositional time of the Caddo Limestone (Figure 26) the karst collapses are indistinguishable on the Sobel Filter Similarity overlay. Despite the subtlety of the karst collapses through the shallower layers the shape index still shows subtle bowl shapes overtop the collapses (Figure 27).

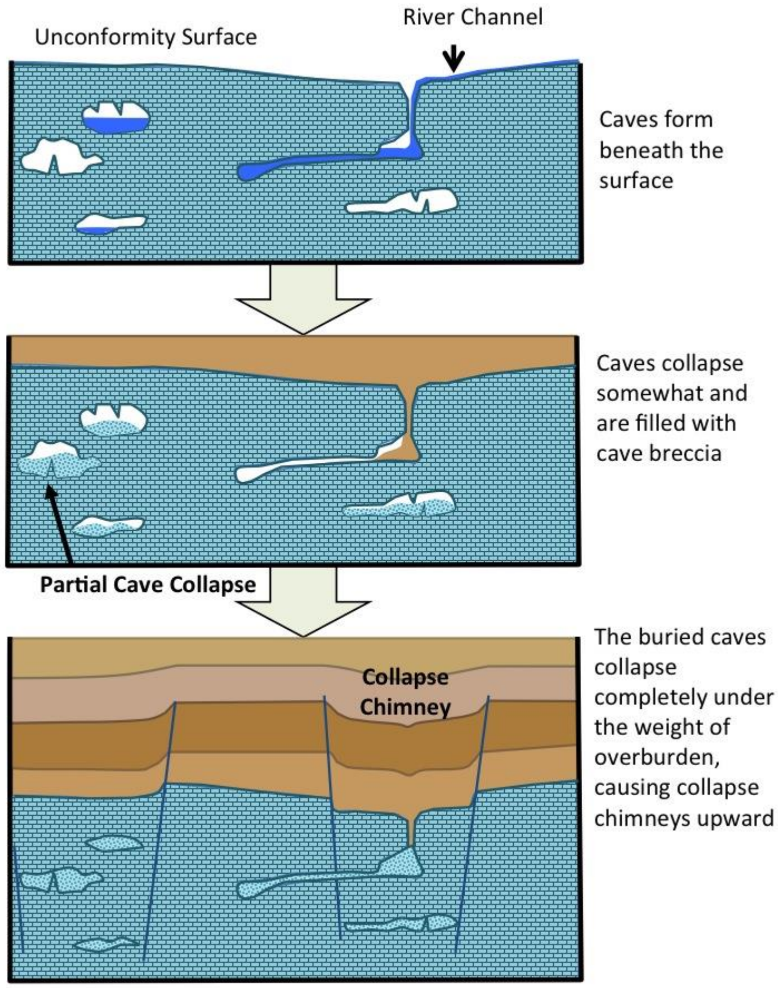

Figure 23. Diagram showing the formation of caves with subaerial exposure, with burial, then collapse of Buried caverns. Based on Tihansky et al. (1999).

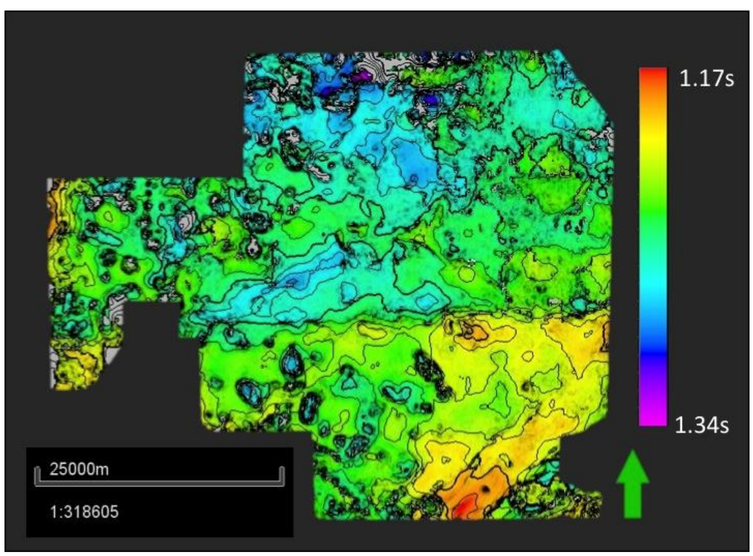

Figure 24. Two-way-time map of the Ellenburger Limestone horizon overlain with the Sobel Filter Similarity. Note the incoherency especially across the western half of the survey.

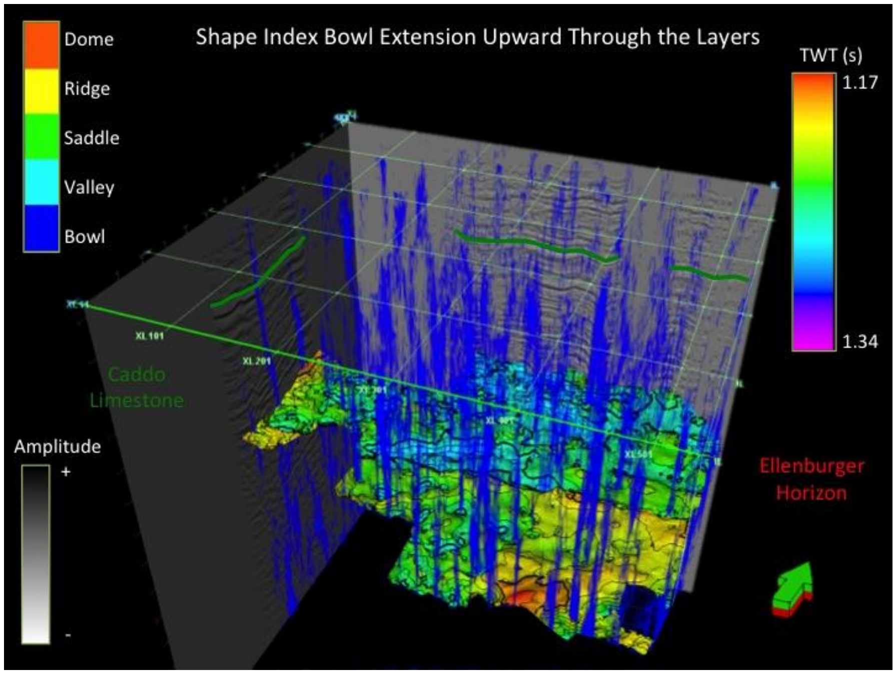

Figure 25: The bowl component of the shape index. These karst collapses extend upward from the Ellenburger horizon, until they decrease in magnitude at the time of the Caddo Limestone deposition.

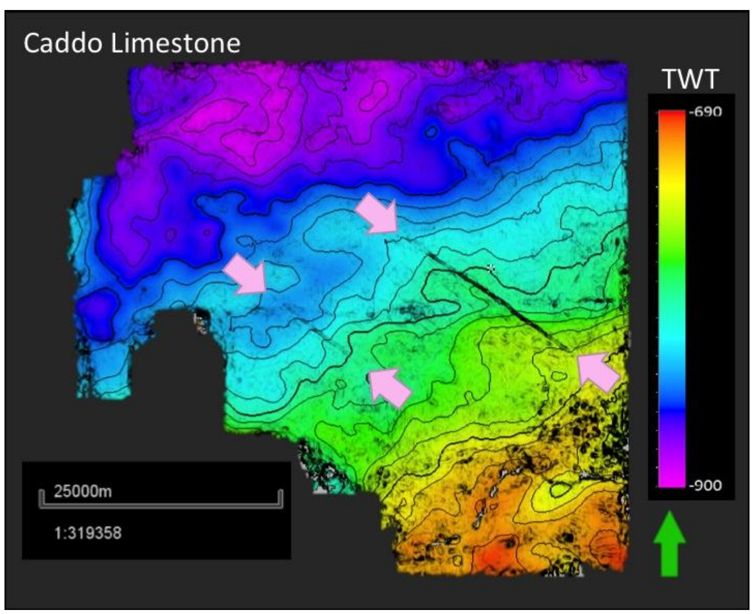

Figure 26. Two-way-time map of the Caddo Limestone overlain with the Sobel Filter Similarity. Note the lack of similarity aberrations representing karst collapses. The fault across the center is barely visible, but

the Riedel shears at Caddo Limestone level are clearly visible.

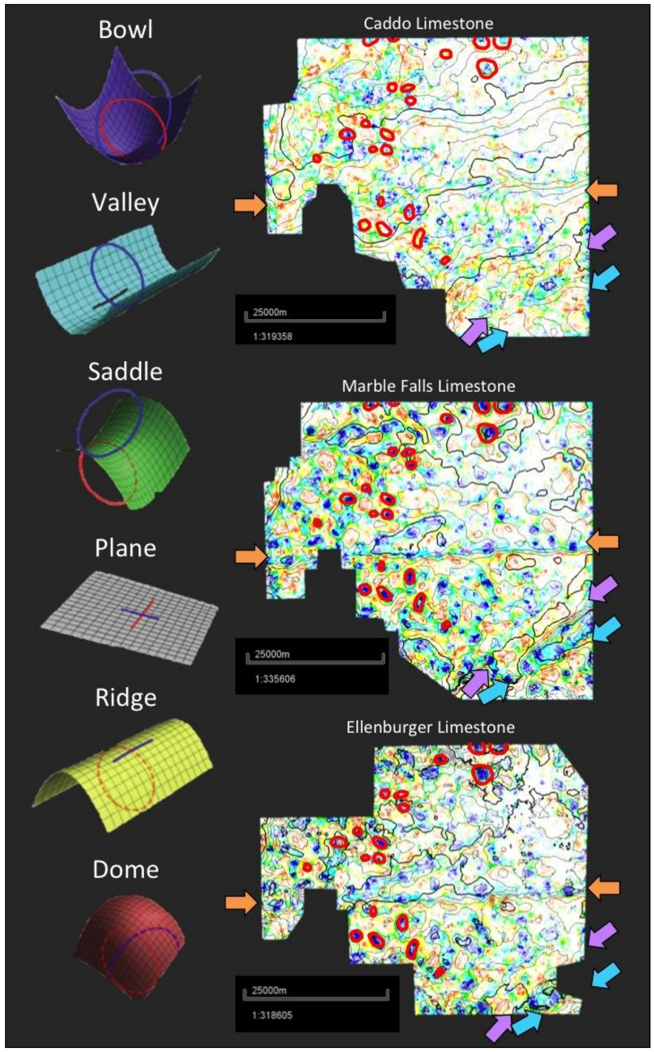

Figure 27. Shape index maps of the Caddo Limestone, Marble Falls Limestone, and Ellenburger Limestone. Several karst collapses are highlighted in red, showing the continuation of the karst collapses through the layers, with the diminishing of the karst collapses by Caddo Limestone time.

The subaerial exposure of the Ellenburger Limestone is especially evident in the subtle channels that Sullivan identified atop the Ellenburger as is seen best in the amplitude gradient (Figure 9). These subtle channels are very difficult to distinguish among the much higher amplitude karst collapses and fractures within the heavily deformed layer.

Sullivan et al. (2006) describe the terrain as characteristic of cockpit karst topography, where dissolution causes collapses while impermeable areas are left as domes. The differential lateral collapse results from dissolution and the "preburial collapse of cave systems" since Sullivan et al. (2006) state "most of the buried Ellenburger cave systems of west Texas collapsed prior to the end of the Ordovician." In contrast, they theorize that the collapses within the survey may be more complex, perhaps representing multiple collapses of Ordovician, Silurian and Devonian cave systems resulting in the around 760 meters of collapse.

The timing of events can be examined by looking at isochron maps, which shows the thickness of a given formation in two-way-time. Since these maps are constructed in two-way-time the effects of velocity must be considered. The velocity of the Ellenburger Limestone on the sonic log is 20,000 ft/s (6,096 m/s), but the brecciated material that collapses to partially fill karsts has a much lower velocity than the original limestone. Having low velocity fill in the karst collapses would cause isochron maps to appear slightly thicker where the karsts occur. If a limestone layer underwent cave collapse while still subaerially exposed sediment deposition overtop would fill downward into the collapses, causing the isochron of the overlying layer to appear much thicker. If the Ellenburger Limestone collapsed before the deposition of the Barnett Shale, that layer would appear much thicker overtop the collapses.

When examining Figure 28 note the distinct karst collapses. The karst collapses at the top are the most distinct on the two-way-time map and have a collapse of about 0.7 s. If the collapses had occurred during the subaerial exposure of the Ellenburger

Limestone, then the Barnett Shale deposition would have filled down into these gaps. Examining the isochron of the Barnett Shale below the two-way-time map we see only slight variations within the circles delineating several karst collapses. There are karsts where the thickness is the same as the surrounding area, yet there are areas where it is thinner and thicker. These variations are much less than the amount of the collapse, indicative that much of the cave collapse occurred after the deposition of the Barnett Shale. Evidence of later collapse is supported by the isochron of the Marble Falls directly above the Barnett Shale. Since the Marble Falls is thicker, the small variations in the time map are smoothed out. In Figure 29 there are no notable thickness changes where the karsts occurred. This means that the deposition didn't infill into the collapses and cause greater time thickness.

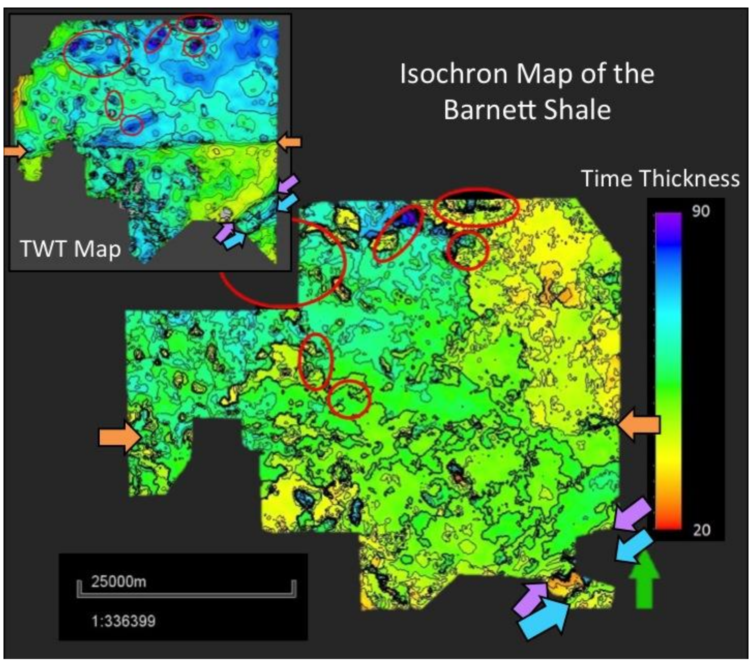

Figure 28. Isochron map of the Barnett Shale. There is no significant thickness change overtop the karsts, which are circled in red. The region within the purple and blue faults is thinner than the surrounding areas.

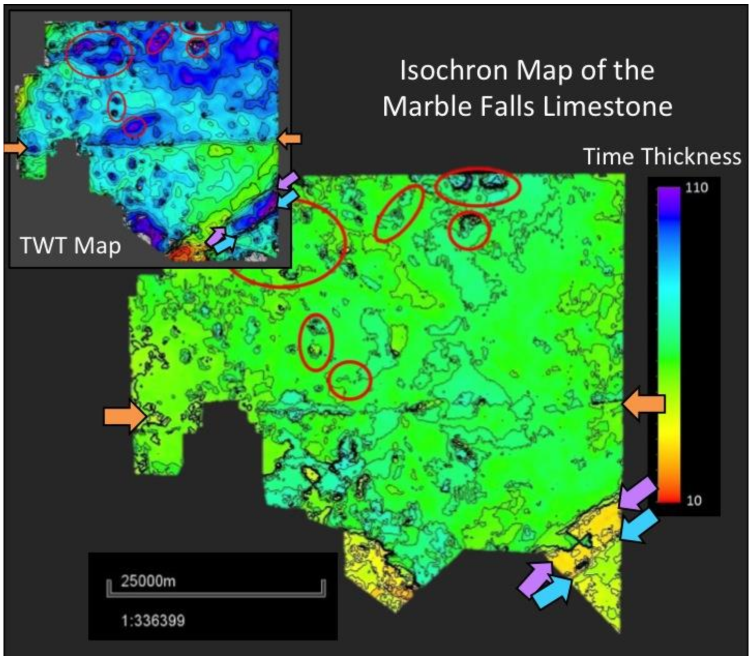

Figure 29. Isochron map of the Marble Falls Limestone. There is also no significant thickness change within the karsts. Thinning is still occurring within the fault system in the southeast. The central fault has a slight mark, but no thickness change.

Midway through the Pennsylvanian Atokan age Bend Conglomerates the karst collapses are less visible, but the depressions they create are still notable. The isochron map of the lower Atokan succession (Figure 30) shows no significant thickness changes either. By the time of Caddo Limestone deposition the karsts became indistinguishable on the overlain Sobel Filter Similarity (Figure 31).

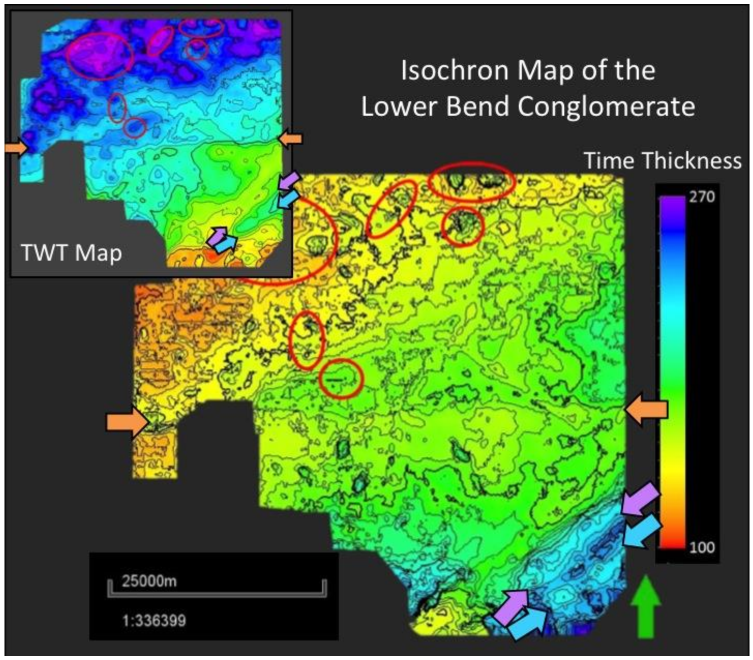

Figure 30. Isochron of the Lower Bend Conglomerates. Note the shift from the previous isochron where the fault system is thickened.

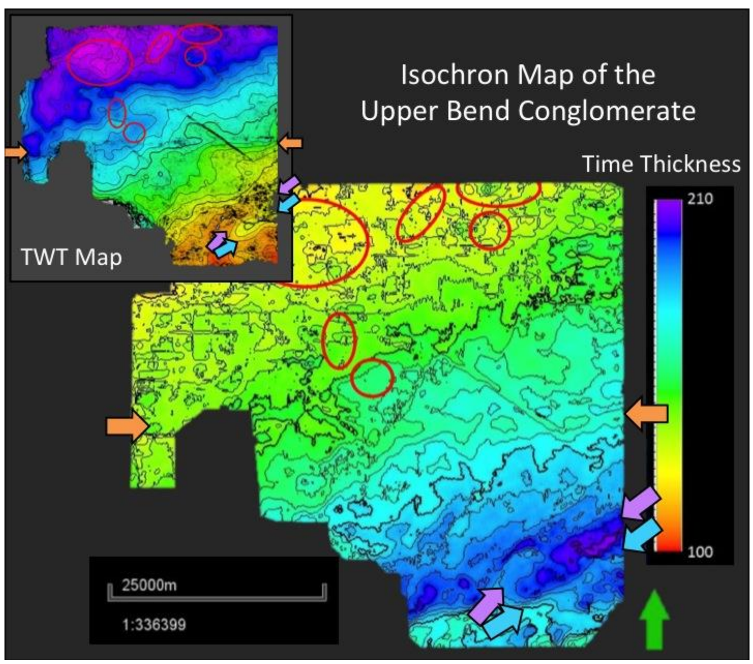

Figure 31. Isochron of the Upper Bend Conglomerates. The region between the graben faults is even thicker than in the lower Bend Conglomerates.

The lack of significant infilling would be explained if the collapses occurred after the deposition of these layers, making these layers have no sharp contrasts in thickness. The subaerial exposure of the Ellenburger Limestone caused caves to form beneath the surface (Figure 23). These caves collapsed as the weigh from the overburden and as the collapses occurred (Figure 32) the mix of sediments from the overlying layers filtered down into the collapse, creating karst collapses that are part subsidence and part collapse sinkholes, resulting in the bowl shape of the collapses that still have a sharp Sobel Filter dissimilarity (Tihansky et al., 2009).

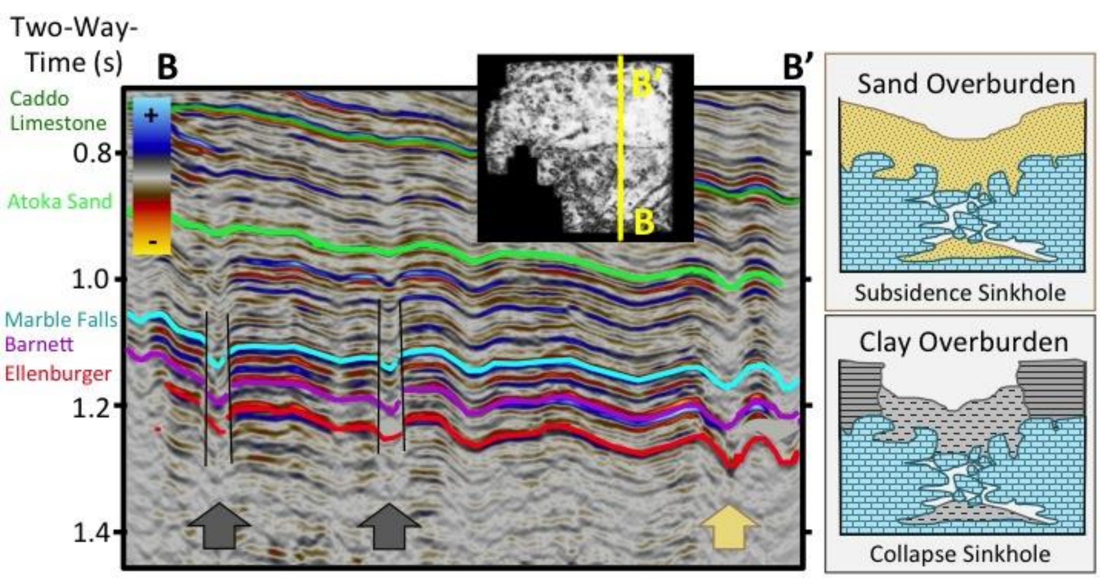

Figure 32. Seismic line BB' through the survey showing the combination of subsidence and collapses that make up karsts within the survey. The Bend Conglomerates have characteristics of both sand and clay overburden. Based on Tihansky et al.'s (1999) analysis of sinkhole overburden in Florida, USA.

Sullivan et al. (2006) theorized that the karsts within the survey are due to a system of faults that extend upward from the acoustic basement. Their interpretation in

Figure 10 shows these faults extending well into the basement, but looking at the layer incoherence displayed in Figure 33 casts doubt on any assumption of a basement faulting connection. The basement in this survey is highly incoherent. Sullivan et al. (2006) interpreted the original seismic volume, where high angle migration artifacts are some of the most linear parts of the basement (Figure 7). Part of the evidence in favor of a connection between sedimentary faulting and basement faulting is the alignment of karst features shown in Figure 34. These lineations persist upward through the layers yet aren't enough to definitively prove a connection. Perhaps, the alignment of collapse features with the regional strain directions at the time is simply a result of cave formation along directions of high strain in the formation at the time of subaerial exposure.

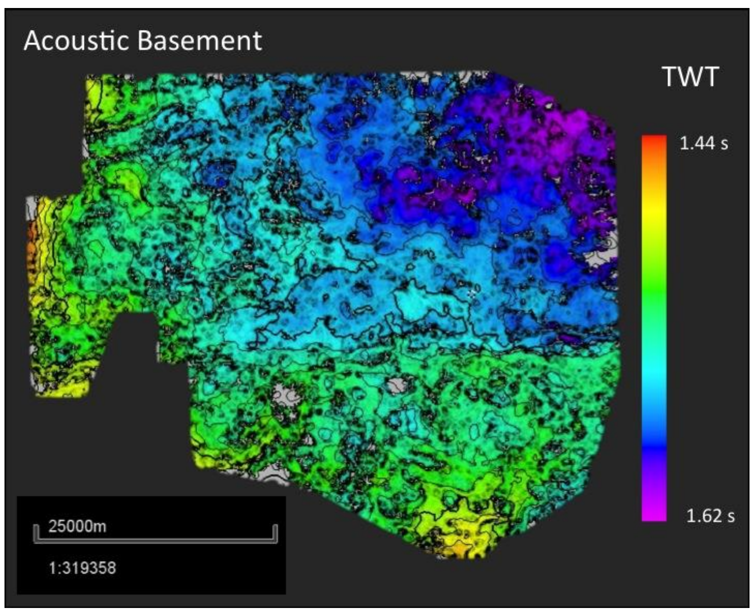

Figure 33: Two-way-time map of the acoustic basement overlain with the Sobel Filter Similarity. Note the lack of similarity across the layer.

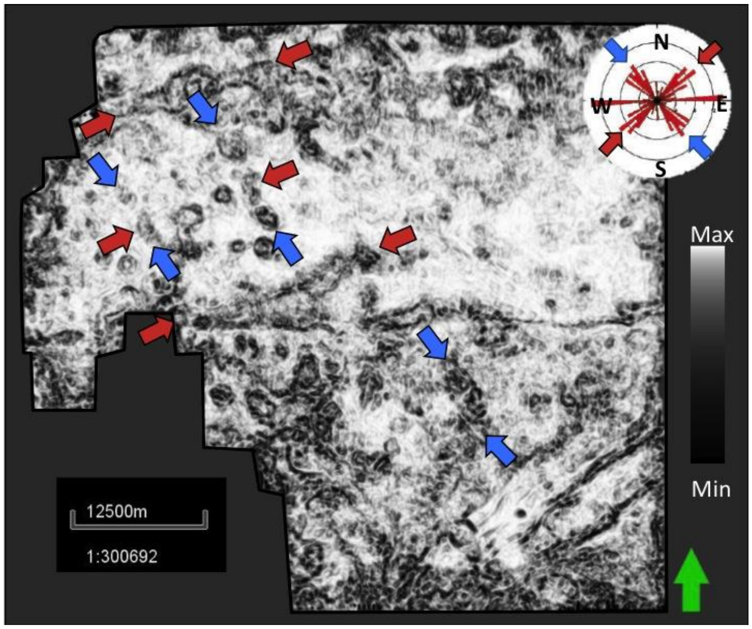

Figure 34. Time slice through the Sobel Filter Similarity at t=1200 at the level just above the Ellenburger Limestone. The strain directions at the beginning of the Mississippian are illustrated in the top right. These lineaments are aligned with the secondary strain directions, shown in blue and red. Strain diagram from Sullivan et al. (2006).

Seismically, the three deepest layers are dominated by the karst collapses, showing very few other stratigraphic characteristics given their low energy depositional environments. Above the Marble Falls Limestone the Atokan age Bend Conglomerates represent the transition to an orogenic belt fluvial deltaic environment. Figure 35 shows the delta systems present for the deposition of the lower Atokan. Southwestern Wise County is within the region of the Decatur fan-delta lobe complex in the upper portion just below the alluvial coastal plain. The Decatur fan-delta complex is characterized by the deposition of coarse conglomerate material. Given the nature of the sediment, the seismic of the lower Atokan sequence has a fairly consistent character, with cleaner conglomerate sand intervals creating these reflectors (Figure 36). These clean sand conglomerate regions create several positive reflections through the otherwise low amplitude seismic.

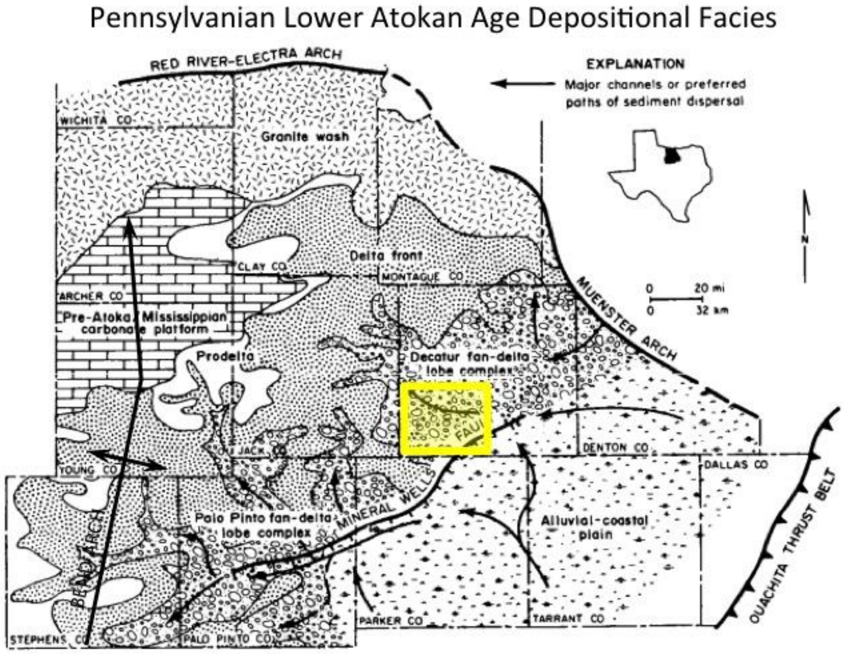

Figure 35. Depositional trends within the northeastern Fort Worth Basin during the early Pennsylvanian Atokan time. From Johnson et al. (1989).

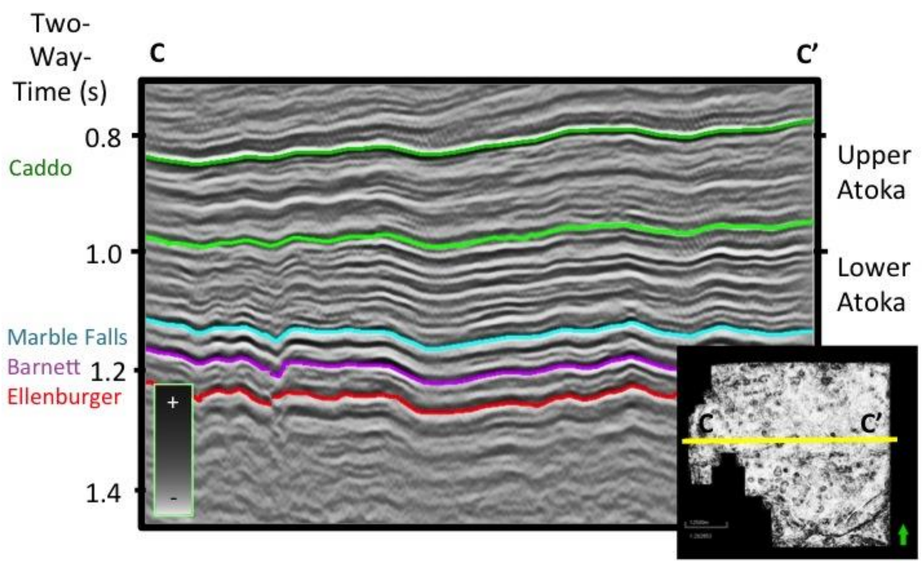

Figure 36. Seismic line CC' showing the more highly incoherent reflectors in the upper Atoka versus the

lower Atoka. In the upper Atoka the layers are largely shale, with very little impedance contrast. The lower Atoka has a mix of clean conglomerates, with some shale layers and some mixed formations, leading to more impedance contrasts and brighter reflectors.

The bright green reflector, labeled Atokan Sand Channel in Figure 36, represents the division between the lower and upper Atokan depositions. The mid-Atokan reflector represents a cleaner sand reflection. Figure 37 illustrates the clearest channel on Sobel Filter Similarity that occurs at around the level of the reflector. This channel runs east to west, at around a two-way-time of 0.978 s, representative of the channels running from the topographic high of the Ouachita Front down into the basin. Above this reflector the data becomes more incoherent. The well log characteristic of the upper Atokan succession is characterized by thick packages of shale with little variation. These shale layers are anywhere from 100 to 250 ft thick, divided by layers of impermeable sandy shale. The lack of acoustic impedance contrasts within the upper Atoka leads to the more incoherent character of the upper Atoka. During the upper Atokan time (Figure 38) the sea level rose locally within the basin as subsidence occurred, causing the delta systems to move further onshore. The shale layers deposited in the southwestern corner of Wise County are just off the delta front.

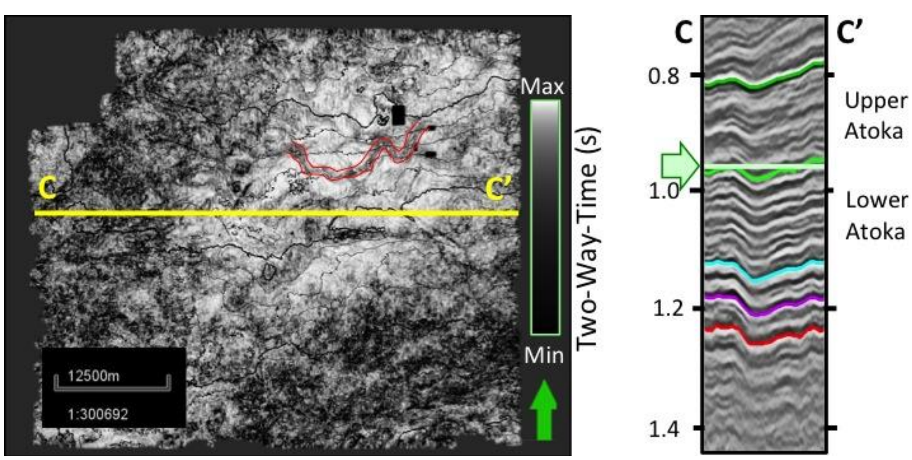

Figure 37. Channel occurring at the boundary between the upper and lower Atokan time. This channel is shown on the Sobel Filter Similarity along a phantom horizon projected 0.158 s below the Caddo Limestone. It flows to the west into the basin.

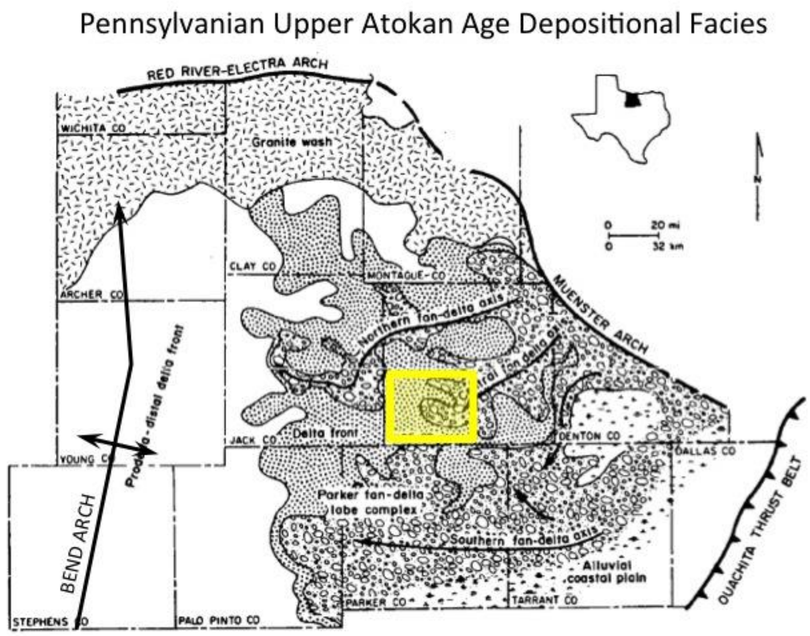

Figure 38. Depositional trends within the northeastern Fort Worth Basin during the late Pennsylvanian Atokan time. Johnson et al. (1989).

The Caddo Limestone is the highest amplitude reflection in the survey. This high amplitude is due to the high impedance contrast between the 12,500 ft/s (3,810 m/s) shale and the high velocity, 20,000 ft/s (6,096 m/s) limestone. The seismic resolution within the survey is just enough that the main reflection is visible, but more detail within the Caddo Limestone isn't visible at the survey resolution. The direction of dip is to the northwest within all the layers, but it isn't until the Caddo Limestone level that the dip becomes pronounced (Figure 39). At the Caddo Limestone level, the dip is around half a degree to the northwest. The further dip at the Caddo Limestone level supports the timing of the basin tilting to the west and north. If the tilting were purely tectonic, the layers would be tilted at the same angle or with deeper layers tilted more. The deepening and tilting that occurred within the basin on the west caused the younger layers, such as the Bend Conglomerates to be deposited fluvially down into the basin. As sea level rose, the Caddo Limestone was deposited atop this slope, leading to the half-degree dip present along this layer. The presence of dip beginning during the deposition of the Bend Conglomerates supports the timing of basin formation during the Pennsylvanian Atokan time.

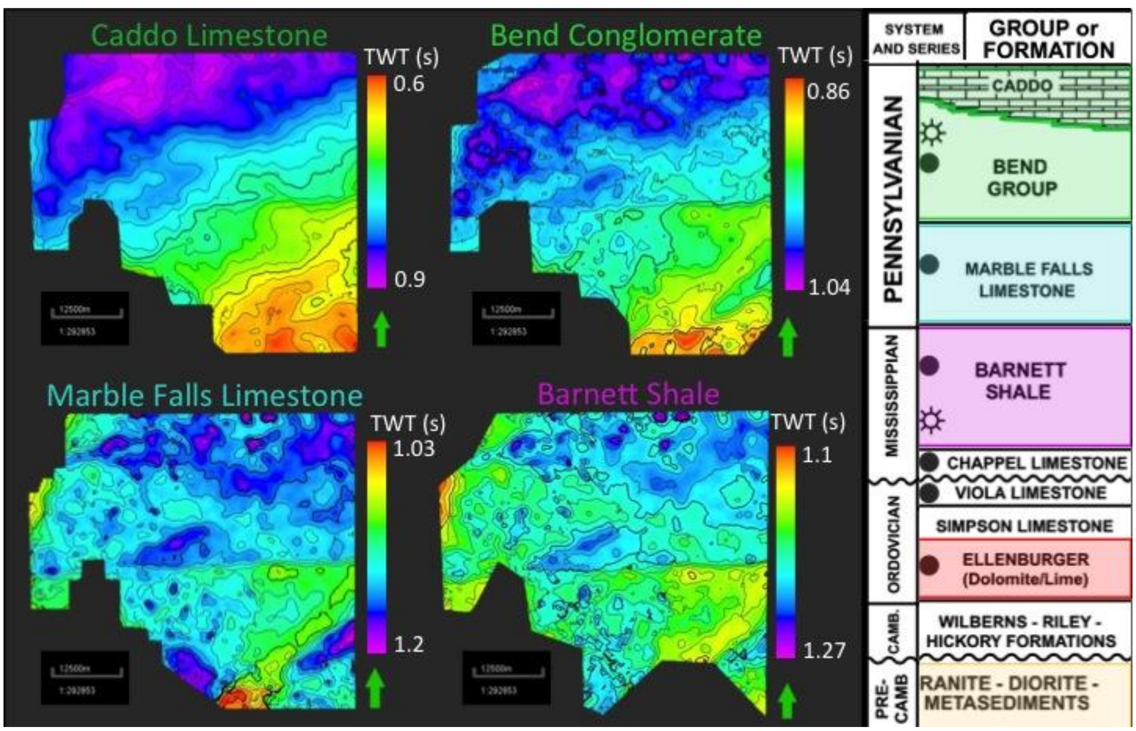

Figure 39. Two-way-time maps through the formations, noting the transition from the flat Barnett Shale, to the Caddo Limestone tilted a half a degree to the northwest.

Above the Caddo Limestone is the rest of the Strawn Group. These layers chronicle the continued westward shift in the basin as the Bend Arch was created. The subsidence and westward shifting deepened the basin as the Ouachita Front progressed, and as the Strawn deposition occurred, the basin underwent northward shifting as well, causing the Bend Arch to plunge to the north. Figure 40 shows a seismic slice through the complete volume. Note the feature outlined in purple, which is a slump feature that begins above the Caddo Limestone and spills down into the basin. The slump feature (Figure 41) begins in the southwestern corner and spills to the north across the survey. The Perrin Delta Complex (Figure 42) began building out into the basin from the Muenster Arch and Ouachita Mountains to the east at the Desmoinsian time. These clinoform features are around 0.12 s thick and outlined in blue on Figure 40. They prograde to the northwest and down into the basin recording the advancement of the delta front.

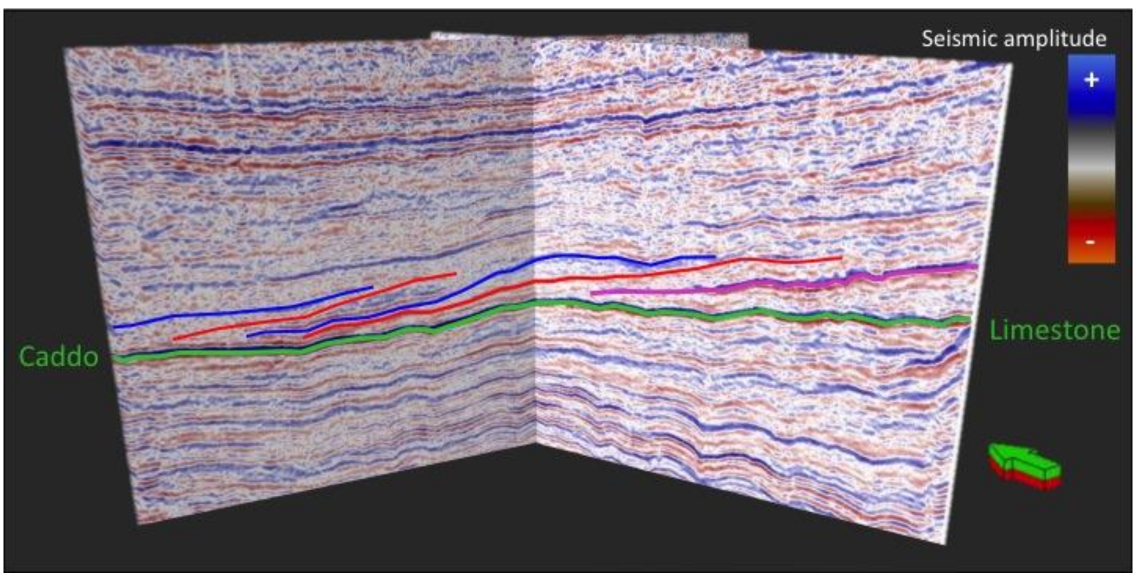

Figure 40. View of the seismic volume from the southwestern corner showing the clinoforms highlighted.

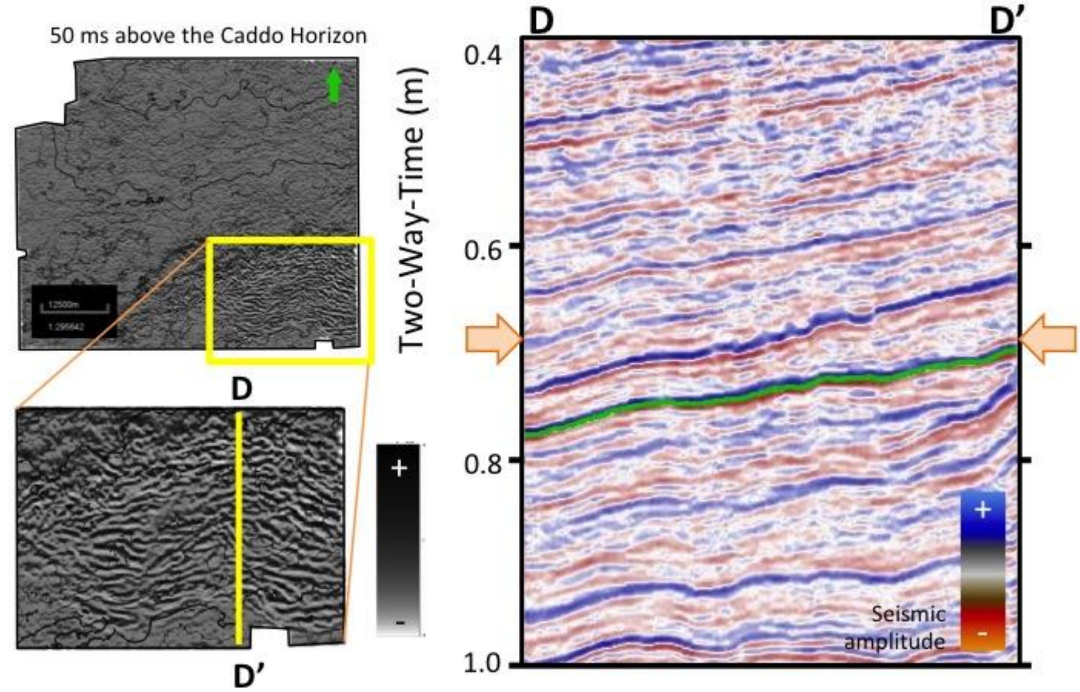

Figure 41. Phantom horizon 0.05 s above the Caddo Limestone just within the clinoforms showing a slump feature originating in the southeastern part of the survey. Line DD' shows the slump feature through the seismic volume.

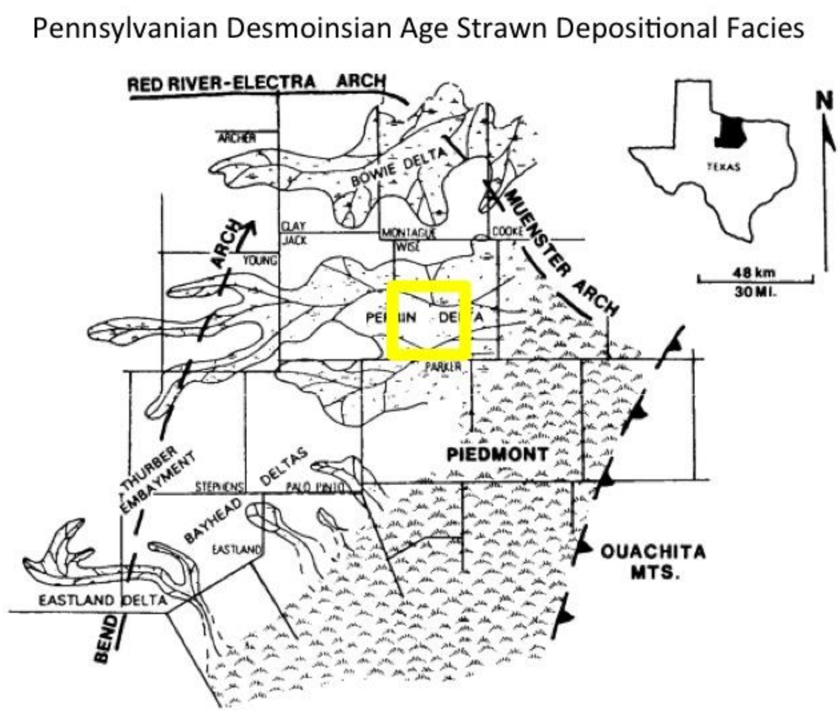

Figure 42. Depositional trends within the northeastern Fort Worth Basin during the Pennsylvanian Desmoinsian time. From Johnson et al. (1989).

The Strawn Group isn't normally a reservoir targeted for hydrocarbon production, but local concentrations of gas and oil do occur within channels. Sand channels that run across the delta front faces have good porosity and permeability and are numerous. Figure 43 shows two channels running northwest along the faces of the prograding delta surfaces. These maps are a co-rendering of RMS amplitude and coherence. Note the high amplitudes that occur within the channels. Commonly, high amplitudes within channels are considered an indicator of gas fill. If a well were drilled into one of these channels and was found to contain gas, then the high amplitude signal could be considered a direct hydrocarbon indicator in other channels with the same high amplitudes within the survey.

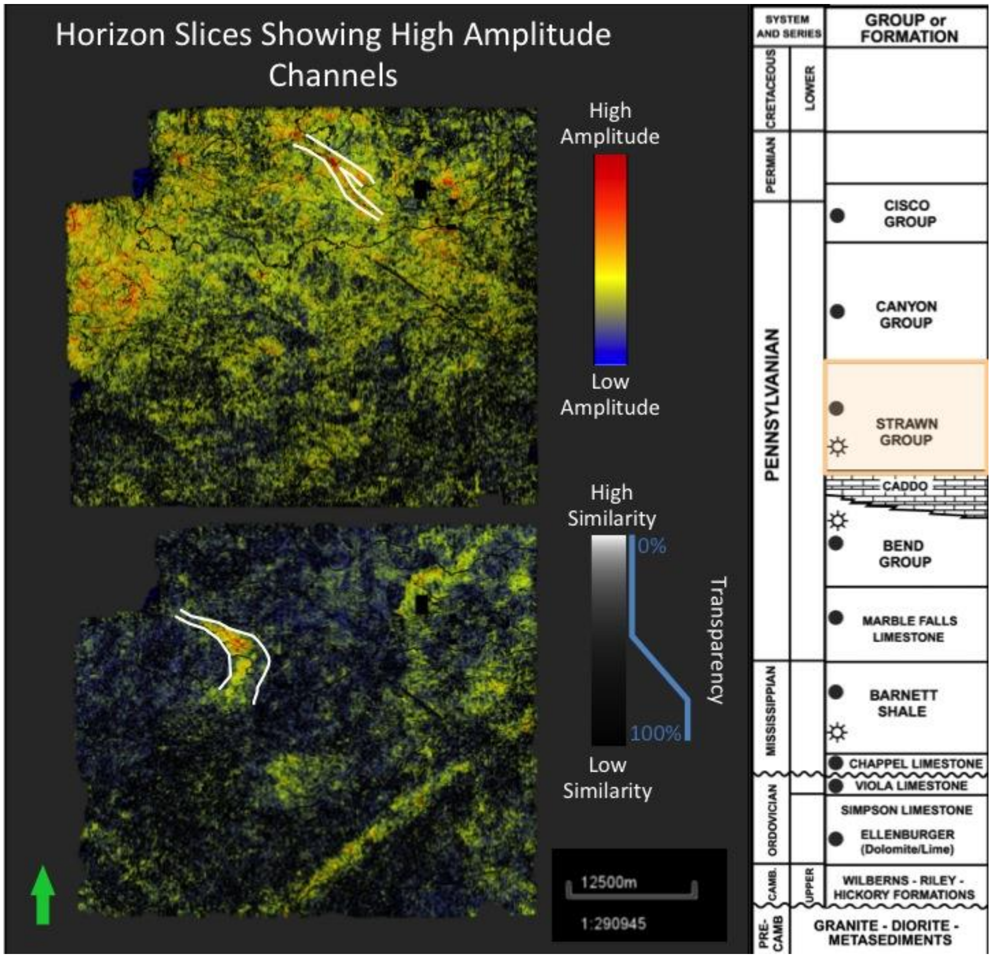

Figure 43. RMS amplitude maps constructed from horizon slices at 0.263 s and 0.208s above the Caddo Limestone. The maps are overlain with the Sobel Filter Similarity. These channels have high amplitudes within the confines of the channel, possibly indicating gas fill despite being so shallow. Both channels flow to the northwest.

By the deposition of the Canyon Group in the Pennsylvanian Missourian time the shoreline had receded to the center of Wise county. The layers atop the progradational delta sequence are somewhat incoherent yet clearly flat lying. They represent the recession of the shoreline back toward the Ouachita Mountains. Several channels occur within these layers above the progradational features, within the Upper Strawn Group (Figure 44). These channels flow to the west, northwest and north, consistent with the direction of deposition at the time.

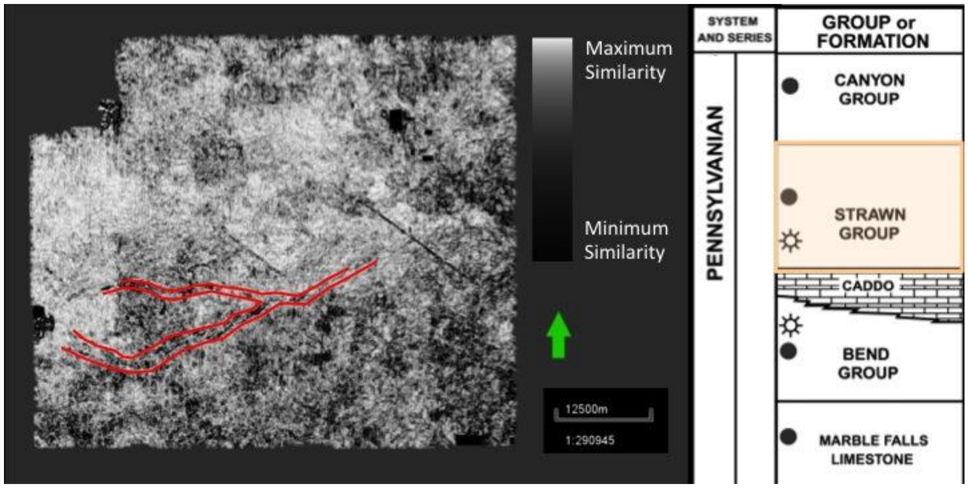

Figure 44. Channel occurring along a phantom horizon slice at 0.288 s above the Caddo Limestone, and flowing to the west.

Through examining the stratigraphic features within the reprocessed and older merged survey the timing of events within the northeastern portion of the basin can be discerned. These events chronicle the westward shift in deposition, the gradual collapse of the Ellenburger Limestone buried cave systems, and the transition from a passive margin ocean to an active fluvial delta system.

6.3 Faulting and Structural Features

Stratigraphic characteristics tell only part of the story, outlining shifts in deposition, erosion and cave collapse. Analysis of the structural characteristics within the survey reveals the changes in tectonic stresses through time.

Faults within the survey are visible on coherence maps and on curvature maps. Coherence maps, such as the one in Figure 12 show the discontinuities along the layer. On Sobel Filter Similarity maps edges are defined as black, with the small circular aberrations being karsts, and the two features marked in orange and light blue being the two main fault systems within the survey. The faults are difficult to see on seismic lines through the survey, but easily distinguished on coherence slices through the volume. Curvature maps, such as the one in Figure 13, show subtle variations in the layer that may be difficult to distinguish on seismic data. Since the faults within this survey aren't sharp contrasts like some, fault scarps can be distinguished on curvature, which is true of both the graben system in the southeast and the large fault across the center.

Sullivan et al. (2006) noted that the orientation of the survey's sedimentary faulting appeared consistent with the regional tectonic setting. Along the northern edge of the basin, the faults run subparallel to the Muenster and Red River Arches and represent a series of fault blocks stepping down into the basin. In the northeastern part of the basin the faults are related to the Mineral Wells Fault System in the area. The Mineral Wells Fault System is a series of older basement faults that were periodically reactivated during the Ouachita Orogeny. The Mineral Wells Fault system is made up of an assemblage of parallel, regionally discontinuous faults. These normal faults trend to the northeast and run directly through the area of the survey (Figure 45). The reactivation of the faults during the Pennsylvanian additionally led to the creation of new faults and graben features trending parallel and sub-parallel to the original system of faults.

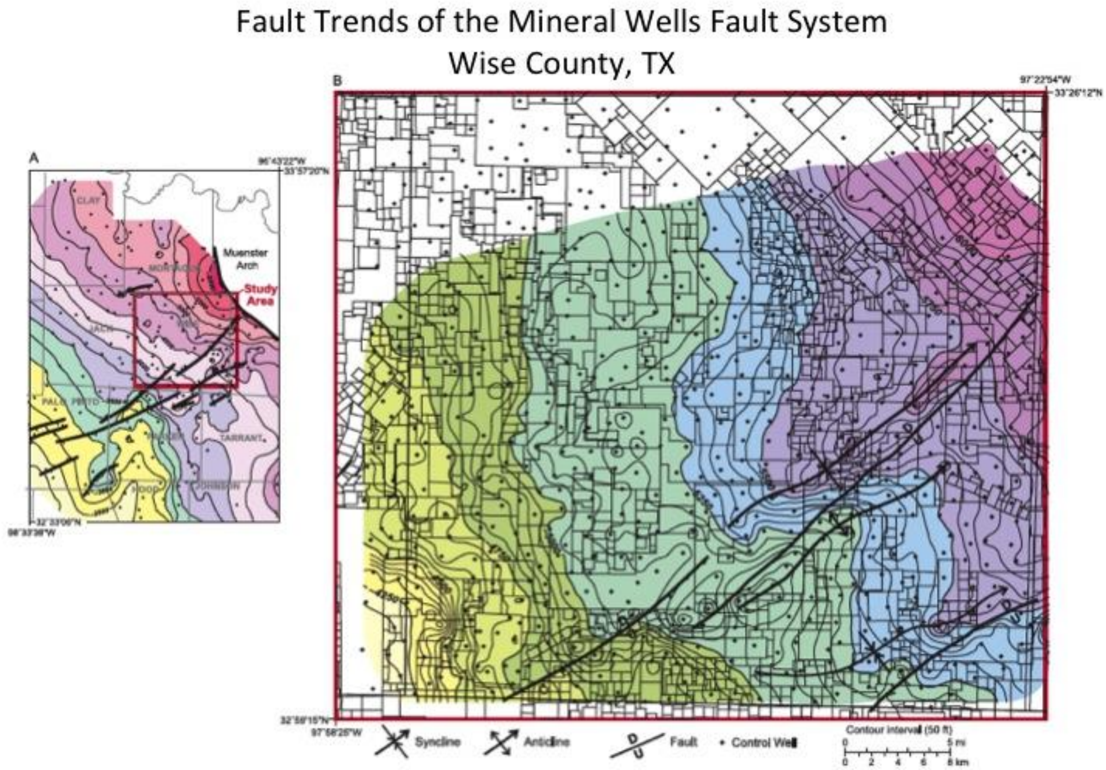

Figure 45. Mineral Wells Fault System mapped through Wise County, Texas. From Hentz et al. (2012).

The survey is characterized by two main fault systems. There is a large strike slip fault running east-west across the center of the survey, which was interpreted to be a strike slip due to the presence of Riedel shear features. The primary strain direction is oriented NW-SE and NE-SW, and the clearest shear features are around 35° from the central fault. They occur in conjugate sets, as can be seen in Figure 46 alongside Sullivan et al.'s (2006) strain diagram. Looking at Figure 47, we see that along a given layer, Riedel shear features open up at distinct angles in response to strike slip motion. This large E-W fault forms part of the Mineral Wells Fault system, with the same block movement and shear component. These discrete faults In Figure 45 are downthrown to the northwest. Looking at Figure 48 you see that the fault is downthrown on the north.

The fault doesn't create a sharp cut across the layers, which would result in a sharp coherence difference (Figure 12), and is instead best seen on curvature maps (Figure 13). The fault scarp appears in the seismic as a 3-mile wide narrow syncline beside a corresponding anticline. A positive curvature anomaly ridge characterizes the upthrown block on the south and a negative curvature anomaly valley characterizes the downthrown northern block. Sullivan et al. (2006) traces these faults downward into the basement (Figure 10) stating that faulting within the basement primarily controls the sedimentary faults. The basement is so incoherent, however, that any appearance of fault continuation into the basement is speculation at best (Figure 49).

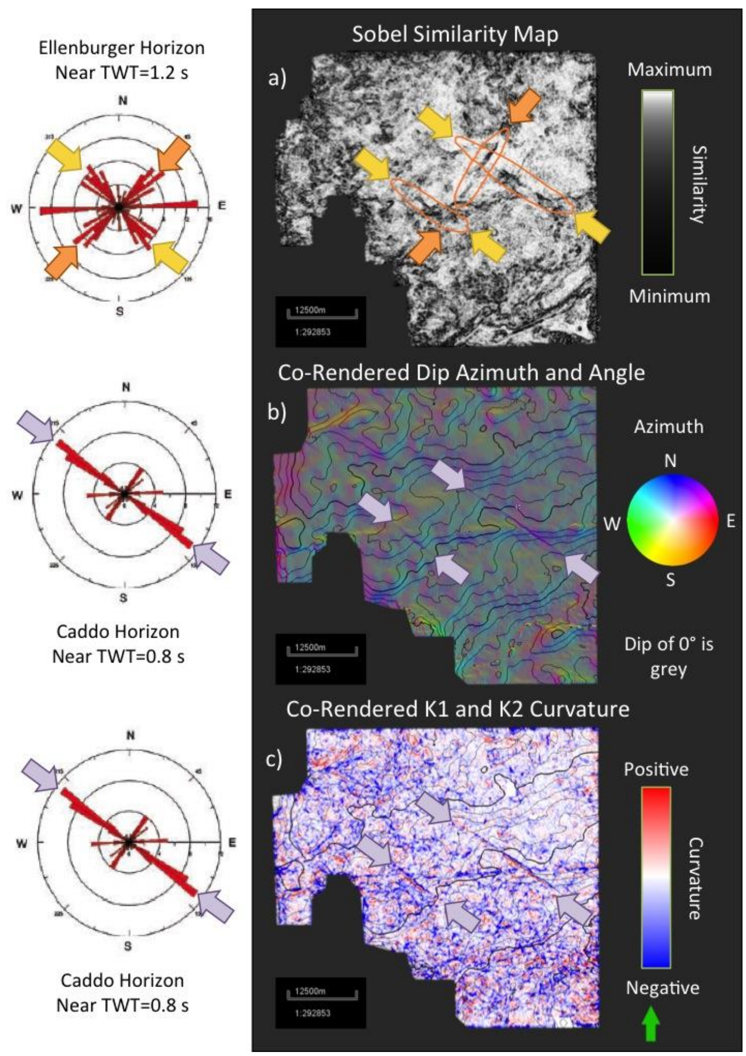

Figure 46. (a) Shows both the Ordovician age strain diagram from Sullivan et al. (2006) on the top left and the Sobel Filter Similarity map of the lower Bend Conglomerates on the top right. Note the shear features that are aligned with the recorded strain directions. (b) and (c) correspond to the strain diagram from the Caddo Limestone horizon. (b) Shows the dip azimuth overlain with the dip angle, with dips of 2° transparent so The azimuth is visible, and opaque for dips of 0° where dip azimuth is irrelevant. (c) Shows the overlain K1 and K2 curvature at the Caddo Limestone level. The shear features are visible as a valley on the right beside a ridge on the left, meaning the little faults have scarps down to the northeast. Strain diagram from Sullivan et al. (2006).

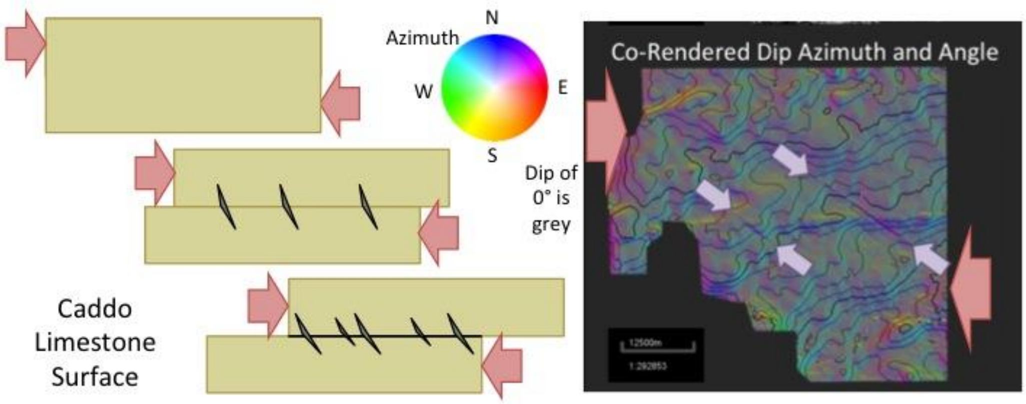

Figure 47. Illustration showing the evolution of Riedel shear features along an evolving right lateral strike slip fault. This similarity in geometry between the model and the gashes along the fault, provides evidence in favor of right lateral movement.

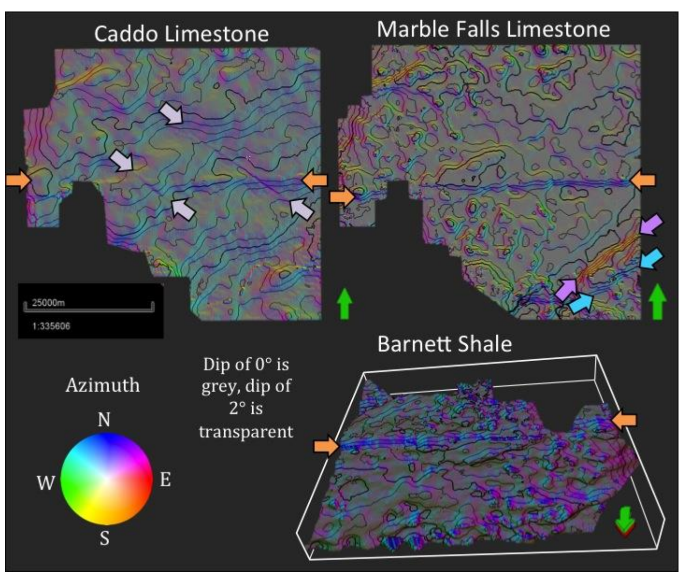

Figure 48. Co-rendered dip angle and azimuth at various formation tops throughout the survey. The dip azimuth color codes the directions of dip along the formation top. The co-rendering of the azimuth with dip angle causes the flat lying areas to be grey, thus eliminating azimuth data on flat layers. Shear features at the Caddo Limestone level are indicated by the lavender arrows, while the large E-W fault through the center is in orange. The graben feature is bounded by the faults in purple and blue. The fault scarp is colored blue, indicating that it dips to the north.

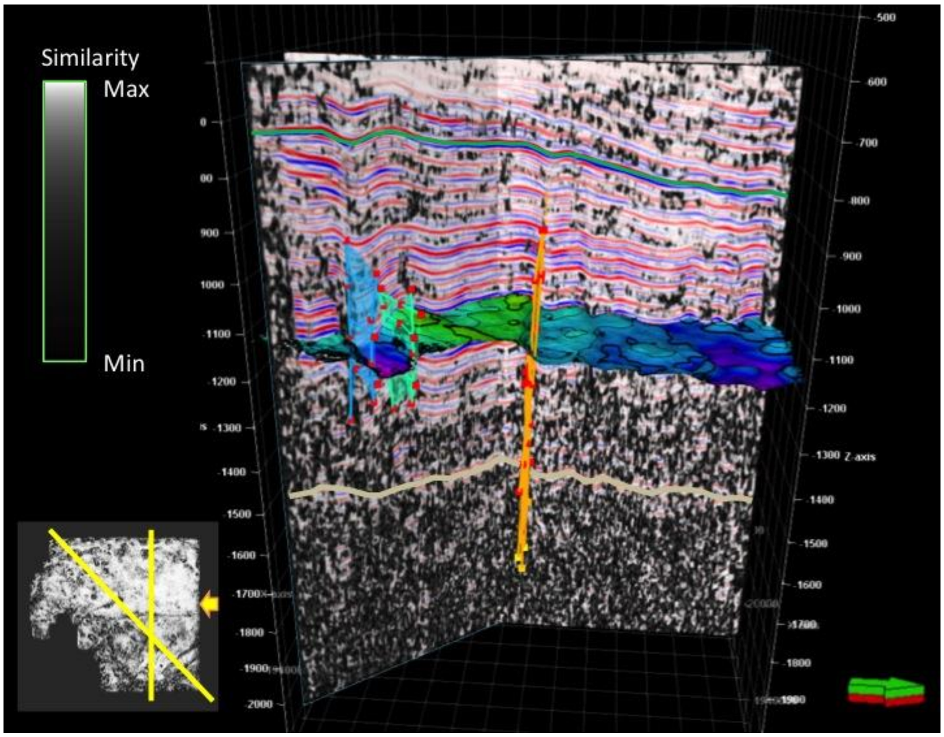

Figure 49. Two slices through the seismic volume, one perpendicular to the graben feature and the other perpendicular to the large E-W fault. The seismic amplitude is overlain with the coherence, showing the incoherence in the basement starting at t=1.3 s.

The lower southeastern corner of the survey has a 1.5-mile wide graben that runs parallel to the Mineral Wells Fault system (Figure 50). The collapse extends from the southern half of the eastern edge four miles to the southwest. It is one of the graben features associated with the Mineral Wells Fault System. Like the other main fault in the survey, the fault may or may not actually extend into the basement. In the future improved data quality due to reprocessing may reveal more detail within the bedrock and prove causality between basement faults and shallower structures.

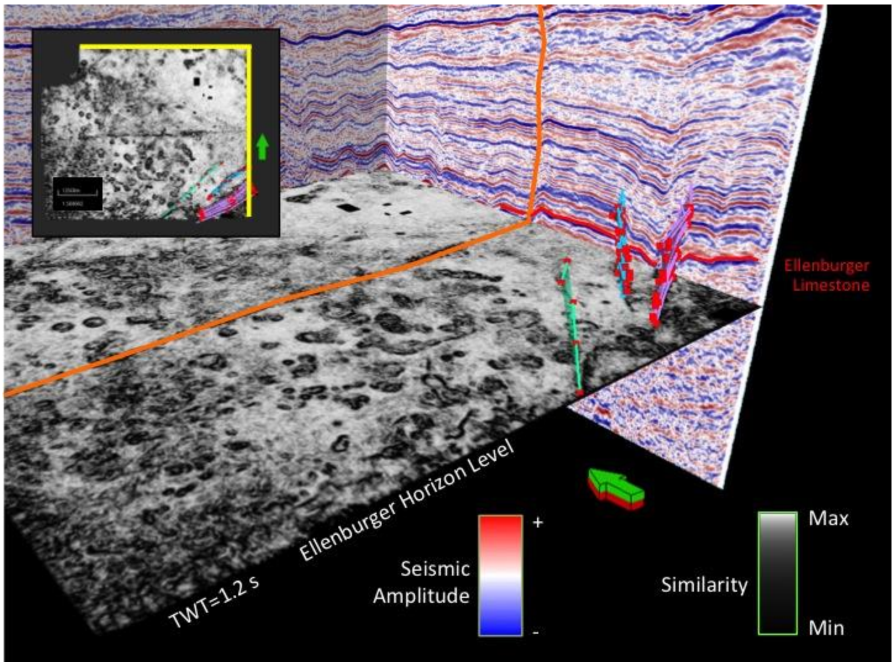

Figure 50. View through the seismic from the southwest. The Sobel Filter Similarity Slice at t=1.2 s is roughly at the level of the top of the Ellenburger Limestone, shows the faults (in color) and karsts as black circles. Note the collapse towards the center of the graben on the slice along the eastern edge.

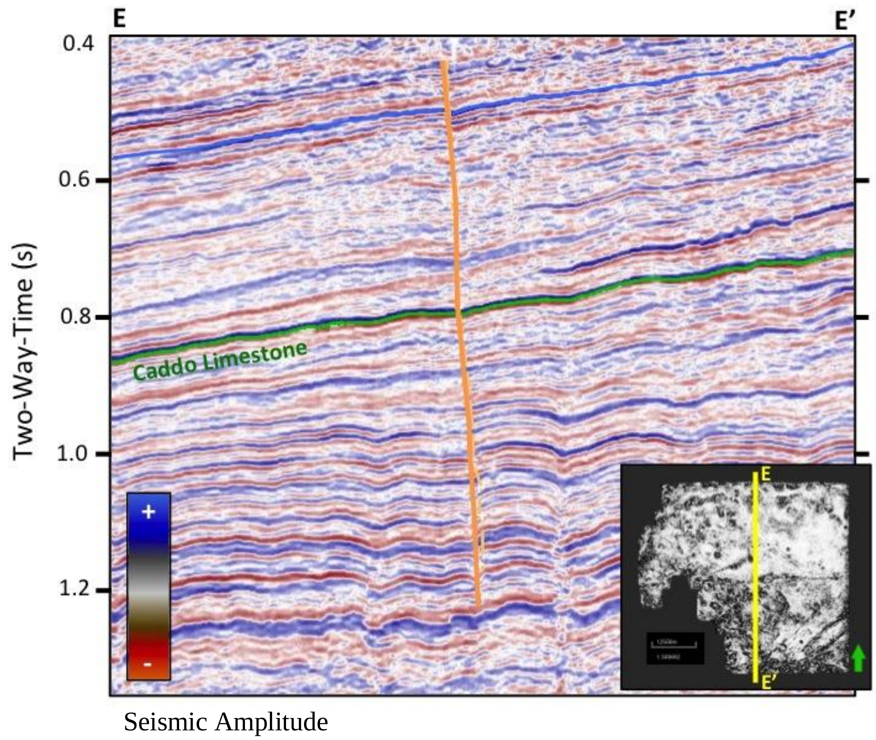

Figure 51. Line EE' through the seismic data showing the continuation of layer thickness across the central E-W fault (orange).

Timing of the fault movement reflects changes in the stress regime in the northeastern portion of the Fort Worth Basin. The timing of both faults are related to the compression and oblique slip associated with the Ouachita Orogeny, then the eventual shift from an environment of compressional collision to passive margin relaxation. The timing of the creation and stress shifts can be determined by examining the isochron maps.

The wrench fault system was created very early in the history of the basin. If the fault movement had occurred after the deposition, then the thickness of the layer would be unperturbed. The isochron map of the Barnett Shale (Figure 28), though lacking some data in the region, has a slight thinning in the area compared to the formation on either side of the feature. This thinning is slight, indicating that some compressional movement occurred during the deposition of the Barnett Shale. This thinning is much more notable in the isochron of the Marble Falls (Figure 29). The compressional movement lifting the horst ended after the deposition of the Marble Falls Limestone. Around the start of the Pennsylvanian Atokan time marks the start of the beginning of the Ouachita Orogeny and compressive force from the east.

The pressure from the east and subsidence of the basin caused “Atokan-age intrabasinal faults [to develop] in response to extensional deformation (Sullivan et al, 2006).” The small fault system in the southeast is part of this system of intrabasinal extensional faults. In the Pennsylvanian Atokan time the faults bounding the block shifted from reverse to normal faults, dropping the block downward. The lower Atokan age Bend Conglomerate is thicker through the graben (Figure 30). This trend of thickness continues into the upward layers as well (Figure 31). The layers at the top of the survey are Pennsylvanian Desmoinsian in age, meaning that the record of stress shifts end at this age. Later extension through the area related to the Miocene age Balcones fault system may have led to further extension and deepening of the graben.

The oblique normal fault that runs east to west across the survey is also related to the Mineral Wells Fault System, but the movement had different timing. The strike slip motion along the fault resulted in the formation of Riedel shear features in conjugate sets along the fault (Figure 47). These features are visible through many of the layers upward through the survey. If the strike-slip motion happened at a certain time, then these Riedel shear features would persist through the layers being moved by fault motion. These shear features are most visible in the Bend Conglomerates and upward into the Caddo Limestone, perhaps due to the jumbled nature of the clinoforms above the Caddo

Limestone. The fault itself is visible through all the layers (Figure 51). Meaning that the motion along the fault was recent enough to cut across all the layers.

Looking at the isopachs of the layers pinpoints the inception of the fault movement. If the fault movement occurred before the layer deposition, then sedimentary deposition would fill onto the downthrown fault block, creating a significant thickness change across the fault. Looking at the two-way-time maps, the drop across the fault surface is around 0.5 s. Analysis of Figure 29, the isopach of the Marble Falls Limestone, shows no thickness change across the fault scarp, indicating the movement occurred after the deposition of the layer. Moving upward to the isochron of the lower Bend Conglomerates (Figure 30) the same is seen. Figure 31, the upper Bend Conglomerates is the best example of layer thickness continuity across the fault. The fact that no thickness differential is visible across the fault means either that the faulting occurred after the deposition or that movement at the time was largely strike slip. Since there are no features that cross the fault surface within the lower layers it is difficult to pinpoint whether the strike-slip component of motion began during the Ordovician through Atokan time or even whether the movement was right lateral or left lateral. However, by examining at the geometry of the Riedel shear features, seems to indicate that the movement was right lateral. This is supported by looking at Elebiju et al’s (2009) Euler Deconvolution Cluster Plot, which has a basement lineation that appears to be offset right laterally (Figure 52). The timing is better pinpointed by looking at the slump feature within the Strawn Group just above the Caddo Limestone. The fact that no offset is visible in this slump feature implies that no strike slip motion occurred after the Desmoinsian time. Seeing that there is are Riedel shear features in the Bend

Conglomerates and Caddo Limestone, but the slump feature has no offset proves that strike-slip motion had to have occurred before the slump was deposited, sometime in the middle Desmoinsian. The slump is also continuous across the fault, not spilling down the front of the fault scarp and causing a thicker region there (Figure 41). This continuity of the slump feature shows that the normal fault movement instigated after the middle Desmoinsian time.

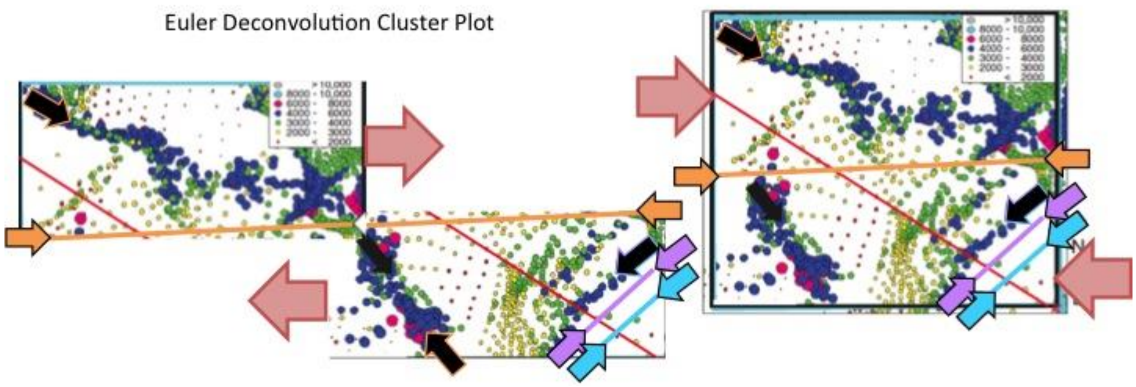

Figure 52. Proposed movement along the central strike slip fault to produce the observed basement gravity alignments. Motion is right lateral. From Elebiju et al. (2009).

Given that the large E-W fault is part of the Mineral Wells Fault System, it has combined portions of strike slip and normal dip slip motion. The basement faulting component of the Mineral Wells Fault System was created before the Ouachita Orogeny, but the sedimentary sequence shows that the strike slip motion occurred before the Pennsylvanian Desmoinsian and was reactivated after it by extensional forces as the basin relaxed after the Ouachita Orogeny.

Chapter 7: Timing and Conclusions

The main control on faulting within the survey and the northeastern region of the Fort Worth Basin is the much older Mineral Wells Fault System. The system of oblique normal faults present in the sedimentary sequence is related to deeper basement faults.

The Ordovician age Ellenburger Limestone was deposited along the passive margin on the southern coast. At Ordovician time there were local faults just over the basement related to the Mineral Wells Fault System. The related faults were compressional horst blocks, as is indicated by the thinner isopach between the bounding faults. During the middle Ordovician the layer became subaerially exposed, leading to channel formation along the top of the layer and the formation of caves beneath the surface.

The horst blocks associated with the Mineral Wells Faults continued to be uplifted During the Mississippian with the deposition of the Barnett Shale and into the Pennsylvanian Morrowan time with the deposition of the Marble Falls Limestone.

The Ouachita Orogeny began in the Pennsylvanian Atokan time. With the stress regime change, many of the faults within the basin were reactivated. The horst block in the southeast was reactivated as well, dropping down to become a graben, indicated by thinning within the fault system (Figure 28 and 29). The small fault blocks were reactivated in response to the extensional forces that oriented in the secondary primary strain direction. At Pennsylvanian Atokan time the basin formed and deepened on the west, causing the westward shift in deposition, leading to the deposition of the jumbled Bend Conglomerates.

Throughout the early Pennsylvanian the weight of overlying layers built up, eventually causing the collapse of the buried caves, creating karst collapse chimneys through the layers with no infilling, leading the isopachs to be of uniform thickness.

Deepening of the basin on the western side continued into the Pennsylvanian Desmoinsian time with the deposition of the Caddo Limestone. Up until Desmoinsian time, strike slip movement had largely characterized the large fault through the center of the survey, evidenced by Riedel shear features in the Caddo Limestone and Bend Conglomerates. This strike-slip motion is consistent with the reactivation of the Mineral Wells Fault System segments during the Ouachita Orogeny. In the Middle and Upper Strawn Group, clinoforms exemplify the westward prograding deltas that dominated the northeastern Fort Worth Basin. Slumped fans within these clinoforms show no lateral offset, illustrating the cessation of the strike slip motion.

Sometime after the compressional environment of the Ouachita Orogeny ceased and the central fault through the survey experienced normal dip-slip movement as the basin relaxed.

The survey serves as a chronicle of the complex geologic history during the Pennsylvanian. With the regional transition from a passive margin, to an active subduction zone, the basin underwent subsidence in response to mountain building on the east. This compressional force led to the reactivation of many older, possibly basement related fault blocks, both small and large. In addition to the large scale uplifts of the Muenster and Red River Arches, smaller associated faults experienced renewed movement. In the northeastern portion of the basin the most influential of these were the faults of the Mineral Wells Fault system. Continued subsidence led to progradation further in the western half of the basin and the formation of large clinoforms. The orogeny eventually ended, the compression ceased, and the most structurally turbulent time in the history of the Fort Worth basin was complete.

Chapter 8: Future Considerations

There is still much work to be done to understand the complete history of the Fort Worth Basin. The next step will be to consider other data along the Mineral Wells Fault system in order to substantiate the exact timing of fault reactivation. The connection proposed by Elebiju et al. (2010) and Sullivan et al. (2006) should be examined as well, using newer vintage data, depth migrated data or a combination of the two.

References

Adams D.C. and G.R. Keller, 1996, Precambrian basement geology of the Permian Basin region of west Texas and eastern New Mexico: a geophysical perspective: The American Association of Petroleum Geologists Bulletin, **80**, 410-431.

Aktepe, S., K. J. Marfurt and R. Perez, 2008, Attribute expression of basement faulting- time versus depth migration: The Leading Edge, **27**, 360-367.

AlHakeem, A. A., 2013, 3D seismic data interpretation of Boonsville Field, Texas: M.S. Thesis, Missouri University of Science and Technology.

Al-Refaee, H. A., 2013, Upper crustal structure of the Llano Uplift: an integrated geophysical investigation: integrated geophysical and geological studies of selected major tectonic features in south central U.S., 50-102.

Ball, M. M. and W. J. Perry Jr., 2004, Bend Arch-Fort Worth Basin province 045: United States Geological Survey.

Berger, Z., M. Boast and M. Mushayandebvu, 2008, The contribution of integrated HRAM studies to exploration and exploitation of unconventional plays in North America: Reservoir, **35**, 42-48.

Blakey, R., 2013, North American paleogeography: Colorado Plateau Geosystems, Inc., http://cpgeosystems.com/nam.html.

Elebiju O. O., G. R Keller, and K. J. Marfurt, 2010, Investigation of links between Precambrian basement structure and Paleozoic strata in the Fort Worth Basin, Texas, U.S.A., using high-resolution aeromagnetic (HRAM) data and seismic attributes: Geophysics, **75**, B157-B168.

Fernandez, A., and K. J. Marfurt, 2013, 3D seismic attribute expression of the Ellenburger Group karst-collapse features and their effects on the production of the Barnett Shale, Fort Worth Basin, Texas: M.S. Thesis, University of Oklahoma.

Hardage, B. A., J. L. Simmons Jr., D. E. Lancaster, R. Y. Elphick, R. D. Edson and D. L. Carr, 1996, Boonsville 3-D data set: Society of Exploration Geophysicists, The Leading Edge, 15, 835-837.

Hentz, T. F., W. A. Ambrose and D. L. Carr, 2012, Reservoir systems of the Pennsylvanian lower Atoka Group (Bend Conglomerate), northern Fort Worth Basin, Texas: high-resolution facies distribution, structural controls on sedimentation, and production trends: The American Association of Petroleum Geologists Bulletin, **96**, 1301-1332.

Johnson, K. S., T. W Amsden, R. E. Denison, S. P. Dutton, A. G. Goldstein, B. Rascoe Jr., P. K. Sutherland D. M. Thompson, 1989, Geology of the southern midcontinent: Oklahoma Geological Society, Special Publication 89-2.

Keller, G. R., M. Khatiwadi and H. Al-Refaee, 2013, The Ouachita Orogenic Belt: some new results and thoughts on its structure and evolution: Geological Society of America, **45**, 84.

Khatiwadi, M., G. R. Keller and K. J. Marfurt, 2013, A window into the Proterozoic: integrating 3D seismic, gravity and magnetic data to image sub-basement structures in the southeast Fort Worth Basin: SEG interpretation, **1**, T125-T141.

Kruger, J. M., and G. R. Keller, 1986, Interpretation of crustal structure from regional gravity anomalies, Ouachita Mountains area and adjacent Gulf Coastal plain: The American Association of Petroleum Geologists Bulletin, **70**, 667-689.

Lin, T. and K. J. Marfurt, 2014, Attribute analysis of the time vs depth-migrated seismic data application to Renqui Field, China: M.S Thesis, The University of Oklahoma.

Loucks, R., 2008, Review of lower Ordovician Ellenburger Group of the Permian Basin, West Texas: Bureau of Economic Geology, The University of Texas at Austin.

Loucks, R. G., P. K. Mescher and G. A. McMechan, 2004, Three-dimensional architecture of a coalesced, collapsed-paleocave system in the lower Ordovician Ellenburger Group, central Texas: American Association of Petroleum Geologists Bulletin, **88** 545-564.

Martineau, D. F., 2007, History of the Newark East Field and the Barnett Shale as a gas reservoir: American Association of Petroleum Geologists Bulletin, **91**, 399-403.

Montgomery S.L., D. M. Jarvie, K. A. Bowker and R. M Pollastro, 2005, Mississippian Barnett Shale, Fort Worth basin, north-central Texas: gas-shale play with multi-trillion cubic feet potential: The American Ass ociation of Petroleum Geologists Bulletin, **89**, 155-175.

Nicholas, R. L. and R. A. Rozendal, 1975, Subsurface positive elements within Ouachita Foldbelt in Texas and their relation to Paleozoic cratonic margin: The American Association of Petroleum Geologists, **59**, 193-216.

Perez, R., O. O. Elebiju and E. Baruch, 2009, Geophysical evidence of basement controlled faulting in the Ellenburger Group and Viola Limestone, Fort Worth Basin, Texas: 79th Annual International Meeting, SEG Expanded Extracts, 995-999.

Pollastro, R. M., 2004, Assessment of undiscovered oil and gas resources of the Bend Arch-Fort Worth Basin Province of north-central Texas and southwestern Oklahoma, 2003: United States Geological Survey National Assessment of Oil and Gas Fact Sheet.

Pollastro, R. M., D. M. Jarvie, R. J. Hill and C. W. Adams, 2007, Geologic framework of the Mississippian Barnett Shale, Barnett-Paleozoic total petroleum system, Bend Arch-Fort Worth Basin, Texas: U.S. Geological Survey, **91**, 405-436.

Reeves, F., 1922, Geology of the Ranger Oil Field, Texas: United States Geological Survey, Contributions to Economic Geology, Part 2, 111-170.

Rodriguez, M. R. D. S. and K. J. Marfurt, 2013, Production correlation to 3D seismic attributes in the Barnett Shale, Texas: M.S. Thesis, The University of Oklahoma

Sullivan, C. E., K. J. Marfurt, A. Lacazette and M. Ammerman, 2006, Application of new seismic attributes to collapse chimneys in the Fort Worth Basin: Geophysics, **71**, B111-B119.

Tihansky A. B., 1999, Sinkholes in west central Florida: Land Subsidence in the United States, United States Geological Survey Circular 1192, 177.

Wright, W. R., 2006, Depositional history of the Atokan succession (lower Pennsylvanian) in the Permian Basin: Bureau of Economic Geology, Jackson School of Geosciences, M.S. Thesis, The University of Texas at Austin.

Zhao, H., N. B. Givens, B. Curtis, 2007, Thermal maturity of the Barnett Shale determined from well-log analysis: AAPG Bulletin, **91**, 535-549.